We are grateful to the editor and referees for their time dedicated to this manuscript and for the constructive comments, which were all taken into account in the revised manuscript. Below, we answer point-by-point all the comments. The comments are reproduced in blue and the authors' responses are provided in black. The responses were coded in **RXCY** format with **X** indicating the referee number and **Y** indicating the referee comment number. The underlined texts are our corresponding changes in the revised manuscript.

The main changes in the revised manuscript include:

- Continuous melt onset (the first day when snowmelt lasts for at least three consecutive days) was added to investigate the pan-Antarctic snowmelt dynamics.
- The introduction section was revised to describe the motivation clearly and concisely.
- The melt detection methods and the evaluation method were described in more detail.
- Uncertainties of the trends were added.
- The comparison between melt extent on the ice sheet and sea ice was removed.
- Figure 5-13 were redrawn, two figures were added as supplements.
- The manuscript was edited by a native English speaker.

Author Response to Referee #1

The presented paper is addressing the melt season in the Antarctic on the Antarctic ice shelves and the Antarctic sea ice cover. The research uses methods for the melt detection from AMSR-E and AMSR2 which are well established and the correction for ice concentration is promising idea to improve the melt onset detection. However, some of the analysis seems shallow and not well documented. Many information on how the results were obtained are missing.

General Comments:

1. The definition of melt is unclear in the manuscript. What exactly is supposed to be detected and discussed?

R1C1: Snowmelt detected by radiometers is actually the presence of snow liquid water (Zheng et al., 2019). We clarified this issue in the revised manuscript:

> Therefore, snowmelt can be detected via microwave radiometry by identifying the sharp changes in microwave brightness temperatures (Tb) caused by the presence of snow liquid water (Serreze et al., 1993; Liu et al., 2005).

Although snow liquid water is produced by surface snowmelt, the presence of liquid water does not always indicate snowmelt. This is because liquid water may remain in snowpack after intense surface snowmelt. However, to be consistent with the previous studies (e.g., Abdalati and Steffen, 1995; Picard and Fily, 2006; Tedesco, 2009; Willmes et al., 2009; Arndt et al., 2016), "snowmelt" is still used in this study. We clarified this issue in Section 5.2 (Uncertainties):

> It should be noted that the presence of snow liquid water detected by AMSR-E/2 does not necessarily mean that the snowpack is melting because it takes time for meltwater to refreeze. In addition, after refreezing of surface snow, subsurface liquid water can still be detected by radiometer due to the penetrating capacity of microwaves (Ashcraft and Long, 2006).

2. Some of the results regarding the melt onset and length are in line with other papers, however the melt onset of sea ice seems quite early in comparison to the cited references and other observations. Thus these early detected melt onset (July, August) need further physical investigation and should probably not directly interpreted as the real melt onset.

R1C2: We thank the referee for this insightful comment.

- Melt onset investigated in this study (the first day that snowmelt is detected) is different from that (the first day when snowmelt lasts for at least three consecutive days) examined in Willmes et al. (2009). In previous studies, the former one was also defined as "early melt onset" (e.g., Semmens et al., 2013; Bliss et al., 2017), while the latter one was regarded as "continuous melt onset" (e.g., Markus et al., 2009) or "persistent melt onset" (e.g., Zheng et al., 2018).
- Early melt onset (EMO) always occurs much later than continuous snowmelt onset (CMO), especially on the first-year sea ice (Fig. R1). Surface melt on the Antarctic sea ice periodically occurs in winter (Massom et al., 2001). In August 2002, early melt events were observed on the first-year sea ice in the Ross Sea, while CMO did not occur until early November (Fig. R1c).

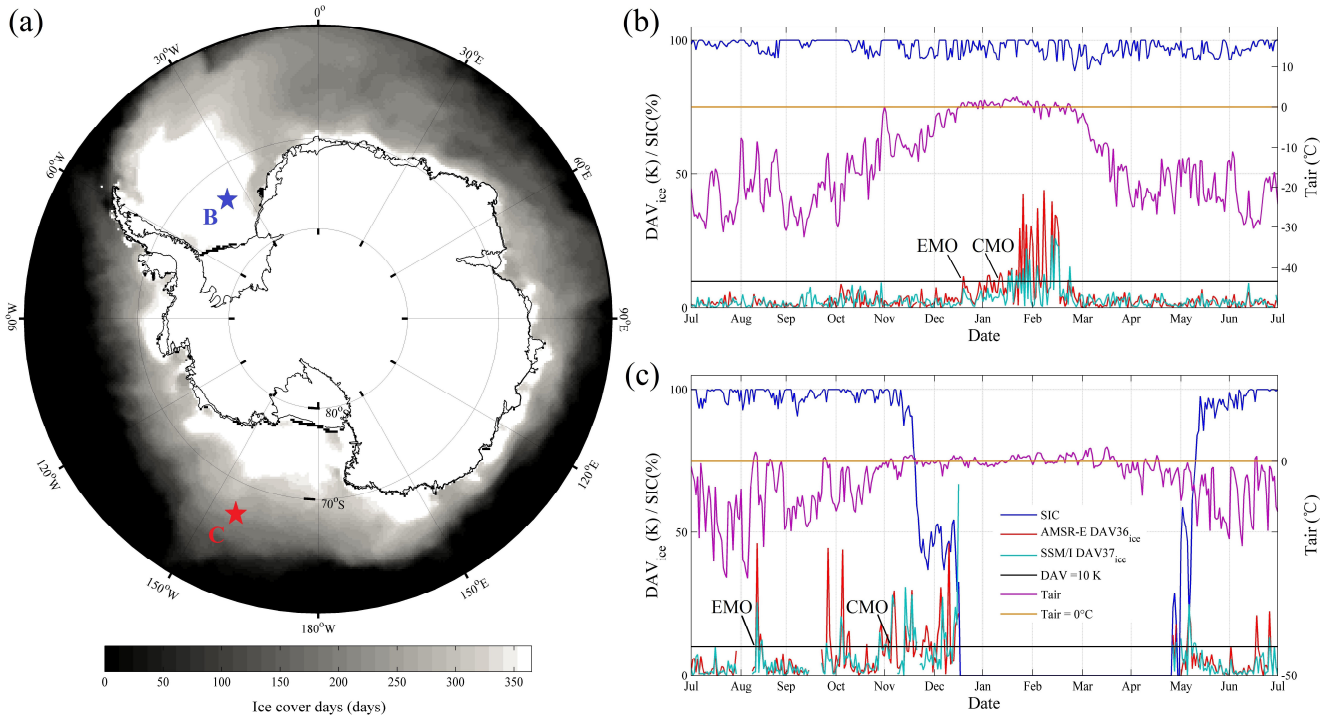

Fig. R1. Surface snowmelt detection on the Antarctic sea ice. (a) Pan-Antarctic ice cover days in 2002-2003, Point B and C show the locations of the pixels examined in (b) and (c). (b) and (c) show the comparisons of sea ice concentration (SIC), ERA-Interim Tair and satellite observations for a multi-year sea ice pixel (Point B) and a first-year sea ice pixel (Point C). $DAV37_{ice}$ and $DAV36_{ice}$ denote diurnal amplitude variations (DAV) of vertically polarized SSM/I 37 GHz Tb and AMSR-E 36.5 GHz Tb contributed by the ice portion, respectively.

- To compare with the results from Willmes et al. (2009) (hereafter W09), CMO was also included in the revised manuscript. Two different kinds of "melt onset" were investigated in this study: Considering the existence of both transient and persistent snowmelt in the pan-Antarctic, early melt onset (EMO, the first day when snowmelt is detected) and continuous melt onset (CMO, the first day when snowmelt lasts for at least three consecutive days) were investigated in this study. On average, CMO was about 53 days later than EMO. CMO derived from AMSR-E and W09 agreed well with each other at high latitudes during 2002-2008. However, AMSR-E found an earlier CMO on the marginal sea ice compared with the results from W09 (Fig. 10). The reasons for their differences were explained:

  First, W09 only studied surface snowmelt on sea ice after 1 October, while the melt season begins on 1 July in this study. Second, the $DAV36_{ice}$ algorithm can amplify snowmelt signals by reducing the effect of open water, so that more melt events can be recognized (Fig. 3). Third, compared

with SSM/I, AMSR-E operated in a stable orbit and observed the pan-Antarctic with more appropriate local acquisition time, and hence had more opportunities to identify melt events (Supplement Fig. 2).

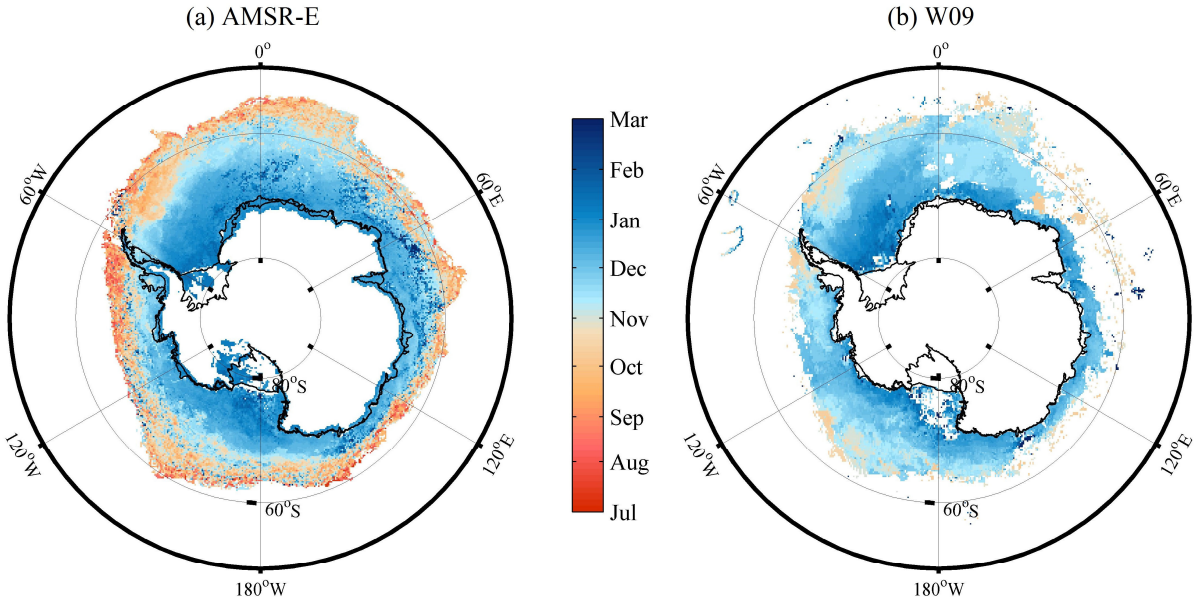

Figure 10. Annual mean CMO derived from (a) AMSR-E and (b) W09 from 2002 to 2008.

3. The optimal local acquisition time of AMSR-E compared to SSM/I repeatedly stated by the authors needs further explanation or investigation. It should be critically discussed whether other influences (maybe sun influences or instrument temperature) can alter the results (lead to too early snowmelt detection)

R1C3: The comparison between SSM/I and AMSR-E Tb observations over dry snow zone suggest the effect of other influences is very limited.

- Dai and Che (2010) have compared the SSM/I and AMSR-E Tb observations, and concluded that the differences between AMSR-E vertically polarized 36.5 GHz Tb (Tb_{V36}) and SSM/I vertically polarized 37 GHz Tb (Tb_{V37}) were small.
- To further examine the interferences from cross-platform, we compared AMSR-E Tb_{V36} and SSM/I Tb_{V37} south of 85° S where surface snow is stable and never melts. R-square between AMSR-E Tb_{V36} and SSM/I Tb_{V37} were both 0.96 for ascending and descending passes during 2002-2003. Bias between the two measurements was only about 1 K. Bias between AMSR-E DAV36V and SSM/I DAV37V were less than 0.4 K. The effect of slight Tb offsets between

different sensors should not affect the melt detection based on temporal Tb variability (Markus et al., 2009).

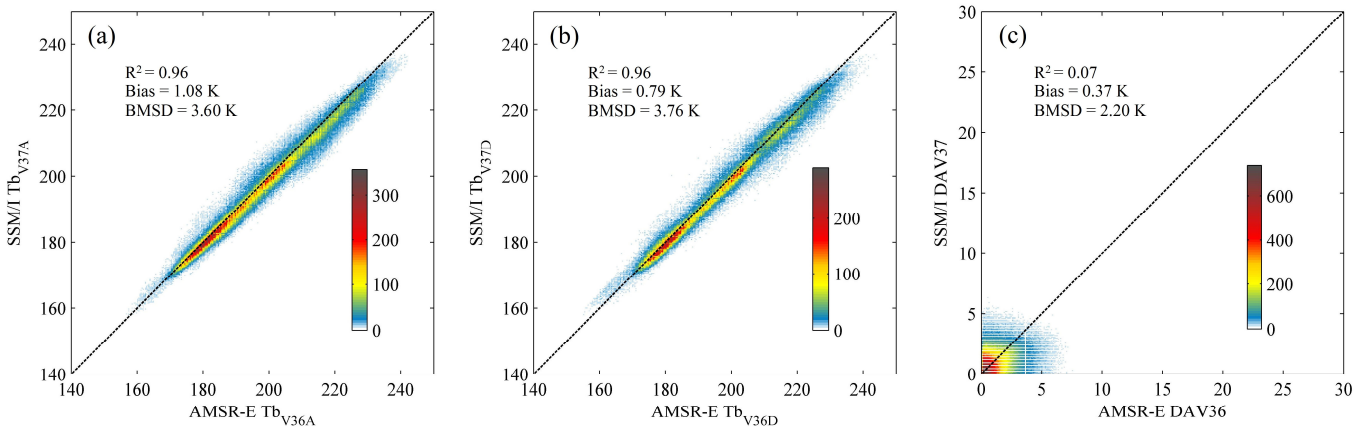

Fig. R2. Comparison between AMSR-E Tb_{V36} and SSM/I Tb_{V37} during 2002-2003. (a), (b) and (c) show the comparisons for ascending passes, descending passes, and the DAV.

- We clarified this issue in the revised manuscript:
  We utilized the same threshold for melt detection based on AMSR-E/2 DAV36 considering the differences between AMSR-E 36 GHz Tb and SSM/I 37 GHz Tb are very small (Dai and Che, 2010). In the region south of 85° S where the surface snow is stable and never melts, the bias between the two measurements was only approximately 1 K during 2002-2003 (Supplement Fig. 1). Slight Tb offsets between different sensors should not affect the results when using temporal Tb variability in melt detection (Markus et al., 2009).

4. I'm surprised to see shelf and sea ice melt in the same way analyzed. They are so different in their nature and also physical properties that I would not even have expected that the same method would work adequately on both. For example there are brine and flooding effects in sea ice which are not present in the shelf ice. It should be more clearly stated in the Manuscript why it is useful or desired to combine the analysis.

R1C4: A uniform approach was applied in melt detection on both the sea ice and ice sheet for two reasons:

- First, snowmelt on the ice sheets was found to be correlated with that on the sea ice, but melt detection on sea ice and ice sheet was always conducted separately. This may result in uncertainties in the integrated study.
  Recent studies (e.g., Ballinger et al., 2013; Stroeve et al., 2017) found that ice sheet atmospheric pattern and snowmelt are linked with sea ice melting conditions through atmospheric circulation.

Earlier melt onset of the sea ice may have provided an additional source of warm, moist air over the adjacent ice sheet, leading to the earlier arrival of melt onset on the ice sheet. However, snowmelt over sea ice and ice sheet was always separately detected with different approaches. In Stroeve et al. (2017), sea ice melt onset was investigated based on Tb temporal variation and gradient ratio following Markus et al. (2009), while the ice sheet melt onset was determined based on a single-channel method following Mote (2007).

In the Antarctic, snowmelt on the West Antarctic and Antarctic Peninsula was also found to be linked with adjacent sea ice variations (Scott et al., 2018; Zheng et al., 2019). So it is worthwhile to generate integrated snowmelt over the pan-Antarctic.

- Second, the DAV method has been successfully applied in melt detection on both sea ice (Willmes et al., 2009) and ice sheet (Tedesco, 2007; Zheng et al., 2018). In addition, the thresholds used for melt detection on the Antarctic sea ice (10 K) and ice sheet (9 K) are very close. A threshold of 10 K works well in melt detection on both sea ice and ice sheet compared with the positive Tair observations (Figure 2&3).

Therefore, this study aims at generating integrated pan-Antarctic surface snowmelt based on the DAV method. We considerably revised the introduction section and clearly clarify the motivations in the last paragraph:

Strong interactions have been found between sea ice and ice sheet surface snowmelt through atmospheric circulation (Stroeve et al., 2017). Surface snowmelt dynamics in the West Antarctic and Antarctic peninsula have been found to be related with the sea ice variations in adjacent seas (Scott et al., 2018; Zheng et al., 2019). Previous studies have separately investigated surface snowmelt on sea ice and ice sheet, which may result in uncertainties in the integrated study. The DAV method has been successfully applied in snowmelt detection on both sea ice (Willmes et al., 2009) and ice sheet (Tedesco, 2007; Zheng et al., 2018). It is worthwhile to estimate snowmelt over the pan-Antarctic based on a uniform approach. The overall objective of this study is to improve the understanding of surface snowmelt over the pan-Antarctic based on the DAV method in three aspects: (1) to detect the pan-Antarctic surface snowmelt at the stable and appropriate local acquisition time based on AMSR-E/2, (2) to improve the performance of the DAV method in the marginal sea ice zone by excluding the effect of open water, and (3) to estimate the pan-Antarctic surface snowmelt as a whole and systematically describe the surface snowmelt patterns and changes from 2002 to 2017.

We acknowledge that brine and seawater flooding could affect the melt detection on sea ice, which was discussed in Section 5.2 (Uncertainties):

Second, although the DAV method used in this study performs well when compared with meteorological observations, the optimal threshold may differ temporally and regionally with varying snow properties. In addition, ice disintegrates, brine and flooding effects may play an important role in seasonal and even diurnal sea ice Tb variations, further complicating the story (Smith, 1998; Willmes et al., 2009).

5. The vast amount of references makes it very hard to find the the real sources for certain statements. This makes the manuscript appear cluttered and lacking a concrete direction and purpose.

R1C5: We thank the referee for pointing out this issue**.** We removed the less relevant references. The introduction was also considerably revised to make the motivations and directions clear.

Some specific Comments:

P1, L16: "DAV" should be directly introduced as TB_v difference of ascending and descending swaths either in the abstract or at the very first occurrence in the text

R1C6: DAV was directly introduced in both the abstract:

In this study, the difference between AMSR-E/2 ascending and descending 36.5 GHz Tb in vertical polarization (DAV36) was utilized to map the pan-Antarctic snowmelt because it is unaffected by the snow metamorphism.

and the text:

Ramage and Isacks (2002, 2003) introduced the SSM/I diurnal amplitude variations (DAV, i.e., the Tb difference between ascending and descending passes) in vertically polarized 37 GHz Tb to investigate the snowmelt timing on the Southeast Alaskan Icefields.

P2, L16 & L23: first statement is "passive microwave remote sensing works in all atmospheric conditions" and then "altered by clouds, atmosphere, …." what do you want to say here?

R1C7: Good catch. Although atmospheric effects are generally negligible in melt detection, they could potentially influence the melt signals and introduce errors (Abdalati and Steffen, 1995). Two avoid contradiction between the two statements, we revised the first sentence:

Microwave radiometers can operate regardless of illumination conditions and are insensitive to atmospheric conditions.

P3, L14: see General point 3.

R1C8: The comparisons between SSM/I and AMSR-E Tb observations over dry snow zone suggest the differences between the two measurements are very small. Please see **R1C3** for full details.

In addition, AMSR-E/2 can observe the pan-Antarctic snowmelt at more appropriate local acquisition time for two reasons:

- First, AMSR-E and AMSR2 operate in controlled-orbits measurements, and the crossing time for the two sensors are nearly the same. By contrast, crossing time differs between SSM/I sensors and also changes significantly over the years of operation due to orbit degradation (Picard and Fily, 2006) (Fig. R3). AMSR-E/2 measurements with a stable orbit are superior in the analyses of inter-annual snowmelt dynamics.

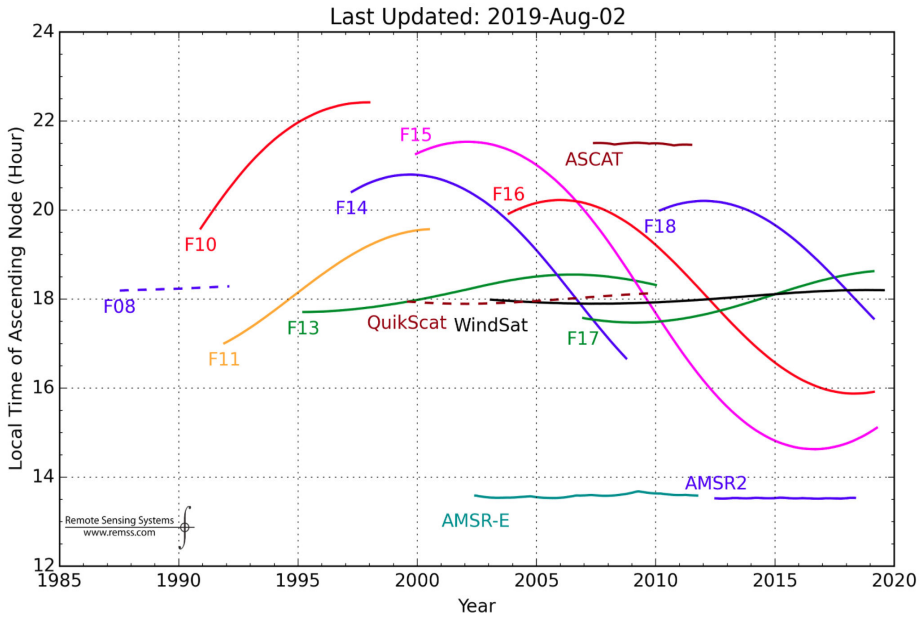

Figure R3. Ascending (solid lines) and descending (dash lines) equatorial crossing times for microwave sensors. The chart is adopted from Remote Sensing Systems (http://www.remss.com/support/crossing-times/).

- Second, the Antarctic diurnal melt area varies approximately as a sinusoid with the peak in the afternoon and the trough in the early morning (Picard and Fily, 2006). It is a great opportunity for us to make full use of the AMSR-E/2 data to detect surface snowmelt because the ascending and descending passes of AMSR-E/2 observed the pan-Antarctic in the afternoon (the warmest period) and at midnight (a cold period).

We rephrased this paragraph to make it clear:

Most of these studies investigated surface snowmelt on sea ice and ice sheets based on SSM/I sensors. However, SSM/I observations show considerable variations in local acquisition time

because of orbit degradation (Picard and Fily, 2006). By contrast, the Advanced Microwave Scanning Radiometer for the Earth Observing System (AMSR-E) and the Advanced Microwave Scanning Radiometer 2 (AMSR2) operate in controlled-orbits so that local acquisition time shows little temporal variation (http://www.remss.com/support/crossing-times). AMSR-E/2 measurements with a stable orbit are superior in the analyses of inter-annual snowmelt dynamics. Diurnal melt area in the Antarctic varies approximately as a sinusoid with the peak in the afternoon and the trough in the early morning (Picard and Fily, 2006). AMSR-E/2 can monitor the Antarctic sea ice and ice sheet (referred to as pan-Antarctic) surface snowmelt at the appropriate local acquisition time. Taking 2002-2003 as an example, the local acquisition time of ascending and descending SSM/I Tb products south of 40° S were 19.17±0.44 and 5.45±0.45, respectively, while these values were 14.16±0.20 and 0.88±0.20 for the AMSR-E Tb products. Compared with SSM/I, AMSR-E/2 have more opportunities to detect melt events in the pan-Antarctic due to warmer and colder periods for ascending and descending passes and an expected higher DAV.

P4, L15: SIC>15% was used and only SIC>80% was used in melt detection? Does this mean a pixel never exceeding 80% SIC is never melting? And pixels exceeding80% SIC only later can only melt from this point on? I would expect that this gives you a negative bias in MDF (since it counts as frozen even in melting conditions).

R1C9: We mean that the pixels with SIC above 80% for less than 5 days (i.e., very short-lived sea ice) were not included in the analyses. That is to say, these pixels were marked as being ice-free (Markus et al., 2009).

- Sea ice pixels and the occurrences of sea ice were first determined, and the melt detection methods were applied henceforth. We employed the same preconditions for melt detection on sea ice based on AMSR-E/2 and ERA. This may not result in the difference in MDF retrieved from the two methods.
- This sentence was rephrased to clarify:
  Pixels with SIC greater than 80% for less than 5 days were marked as being ice-free (Markus et al., 2009). For a sea ice pixel, SIC above 15% indicates the presence of sea ice (Meier and Stroeve, 2008).

P4, L20: please state the exact field of the ERA interim dataset used including timestep, are you using "Air temperature at 2m height" from the surface analysis? Also: in how far was the data used to "assist" with the AMSR-E/2 melt detection? Is this is described somewhere else in the text?

R1C10: We revised this sentence to clarify:

The 6-hourly air temperature (Tair) from the gridded ERA-Interim reanalysis at 2 m height was used to...

Yes, in Section 3.2 (Melt detection methods), we clearly described how the ERA-Interim Tair was used.

- First, ERA-Interim Tair was used to assist with melt detection based on AMSR-E/2:
  Further, melt detection was constrained to the days with compatible thermal regimes following Belchansky et al. (2004). The days with ERA-Interim Tair > -5°C were first determined, and the DAV36 algorithm was applied henceforth.
- Second, ERA-Interim Tair was also used to determine snowmelt directly:
  To evaluate the performance of the DAV method on a larger scale, snowmelt over the pan-Antarctic was also determined by ERA-interim reanalysis when the daily maximum Tair exceeded -1°C.

P4, L29-P5: It is unclear what the MEMLS simulation is for. In Kang et al. (2014), which you are citing four times in this paragraph, this is discussed in very detail. The variation of snow grain size is barely discussed in this paragraph and from what I got, never really picked up again in the manuscript. I would probably just remove the Fig. 1.

R1C11: We recalled the work from Kang et al. (2014) to show that the DAV method is superior to single-channel methods in snowmelt detection. In Willmes et al. (2009), the DAV method was only applied in the detection of snowmelt onset on sea ice. The analysis with varying snow grain size was added to explain that the DAV method can be used to detect snowmelt throughout the melt season with snow metamorphism:

- In early melt season, Tb_{V36} of the fine-grained snowpack increases rapidly in energy saturation phase with a slight amount of liquid water. Daily Tb variations are large because of the contrasting freeze/thaw state. DAV method can recognize these sharp changes.
- During the melt seasons, snow grain size can increase to 2 mm when meltwater refreezes in the pore space (Winebrenner et al., 1994). Tb_{V36} from a melting snowpack may be even lower than the winter mean due to the enhanced volume scattering, and single-channel methods may fail to work (Zheng et al., 2018). By contrast, significant daily Tb_{V36} variations still exist in the transition from dry to wet snow regime in the coarse-grained snowpack, and the DAV method still works.

Fig. 1 illustrates the advantage and principle of DAV method in melt detection. We revised this section to clarify the necessity of this figure:

Tb_{V36} of the fine-grained snowpack increases rapidly in the energy saturation phase with a slight amount of liquid water, and daily Tb variations are large because of the contrasting freeze/thaw

state. Therefore, both single-channel and DAV methods can recognize these sharp changes in the early melt season. During the melt seasons, snow grain size can increase to 2 mm when meltwater refreezes in the pore space (Winebrenner et al., 1994). As a result, Tb_{V36} of the coarse-grained snowpack is much lower than that of the fine-grained snowpack due to enhanced volume scattering. Single-channel methods may fail to work when the Tb_{V36} of a melting snowpack is even lower than the winter mean in the late melt season (Zheng et al., 2018). By contrast, significant daily Tb_{V36} variations still exist in the transition from a dry to wet snow regime during the heavy melt season, even when day-time Tb_{V36} is in the energy dampening phase (Fig. 1). Diurnal freeze-thaw cycles are prevalent in polar regions (Hall et al., 2009; Willmes et al., 2009; van den Broeke et al., 2010b). The simulations suggest that the DAV method can detect melt signals for both the melt onset (e.g., Willmes et al., 2009) and the entire melt season when diurnal freeze/thaw transition occurs (e.g., Zheng et al., 2018). Moreover, the optimum acquisition time of AMSR-E/2 enables us to take full advantage of the DAV method in melt detection.

P5, L5-6: specify the interface you are talking about, probably the snow-air-interface

R1C12: Done! Yes, we mean the snow-air interface.

P5, L10-15: Since you employ the method, can you show that this signal is consistent characteristic for melt? For a longer constant melt under full sun illumination, there is probably not much difference between day and night wetness in the snow. Also in Fig. 3, under constant positive air temperatures, there is not constant DAV>10 which indicates that the melt indicator from DAV and the positive temperatures are not strictly connected.

R1C13: Yes, positive Tair can only provide evaluation rather than validation of the melt detection methods. Considering the absence of in-situ snow wetness measurements in polar regions, positive Tair was always used to evaluate satellite-derived snowmelt because the occurrence of surface melt corresponds to the spatial pattern of Tair (Tedesco, 2009; Liang et al., 2013). However, melt signals (i.e., the presence of snow liquid water) detected by AMSR-E/2 do not always strictly connect with positive Tair for the following reasons:

- First, positive Tair was derived from the hourly Tair measurements from AWS, while AMSR-E/2 only provide twice-daily observations, which may miss the time when melt occurs.
- Second, passive microwave sensors detect liquid water rather than snowmelt. It takes time for meltwater to refreeze after intense melt events. Subsurface liquid water may remain after the refreezing of the surface, and can still be detected by the satellites due to the penetrating ability of microwave (Zheng et al., 2019).

- Third, owing to the penetration and absorption of solar radiation within the snowpack, snowmelt may occur when Tair is below the freezing point (Koh and Jordan, 1995).
- Last, the DAV method may fail to detect snowmelt when liquid water does not refreeze or snowpack is still melting in warm nights (Willmes et al., 2009).

In the revised manuscript, we explained the reasons why satellite-derived melt signals and the positive Tair are not strictly connected:

> Melt signals derived from the DAV method and the positive Tair from AWS were not always strictly connected (Figs. 3&4). Their differences may be attributed to inconsistent temporal resolutions because snowmelt and refreezing can occur at any time of the day. The daily maximum Tair was derived from hourly Tair records, while only two daily satellite observations were used in the DAV method. In addition, snowmelt may occur when Tair is below the freezing point because of the penetration and absorption of solar radiation within the snowpack (Koh and Jordan, 1995).

The limitations of the DAV method were also clarified:

> There are several uncertainties in the pan-Antarctic snowmelt derived from AMSR-E/2 data. First, the DAV method may fail to work when liquid water does not refreeze or snowpack is still melting in warm nights (Willmes et al., 2009). The regions with snowmelt that became more prevalent would presumably show a decrease in melting days based on the DAV method. Fortunately, unlike the Arctic, surface snowmelt on the Antarctic sea ice is always patchy and relatively short-lived (Drinkwater and Liu, 2000). Second, although the DAV method used in this study performs well when compared with meteorological observations, the optimal threshold may differ temporally and regionally with varying snow properties. In addition, ice disintegrates, brine and flooding effects may play an important role in seasonal and even diurnal sea ice Tb variations, further complicating the story (Smith, 1998; Willmes et al., 2009).

P5, L15: see General point 3.

R1C14: The differences between AMSR-E Tb_{V36} and SSM/I Tb_{V37} are small (Dai and Che, 2010). The comparisons between SSM/I and AMSR-E Tb observations in the dry snow zone suggest the effect of other influences is very limited (Fig. R2). AMSR-E/2 DAV36 is superior to SSM/I DAV37 in melt detection because of the more stable orbit and more appropriate acquisition time. Please see **R1C3** and **R1C8** for full details.

P5, L21: see General point 3.

R1C15: The differences between AMSR-E Tb_{V36} and SSM/I Tb_{V37} are small (Dai and Che, 2010). The comparisons between SSM/I and AMSR-E Tb observations in the dry snow zone suggest the effect of other influences is very limited (Fig. R2). AMSR-E/2 DAV36 is superior to SSM/I DAV37 in melt detection because of the more stable orbit and more appropriate acquisition time. Please see **R1C3** and **R1C8** for full details.

P5. L31: I cannot see this in Figure 2. There are at least 3 years (2005, 2007,2009) where there is day in mid-winter with positive air temperature where DAV does not exceed the threshold nor shows any signal.

R1C16: Positive Tair and snowmelt are short-lived in winter. Positive Tair was derived from the hourly Tair measurements from AWS, while AMSR-E/2 only provide twice-daily observations, which may miss the short-lived melt events because refreezing can be quasi-instantaneous in the Antarctic (van den Broeke et al., 2010a).

Positive Tair can only provide evaluation rather than validation of the melt detection methods. Considering the absence of in-situ snow wetness measurements in polar regions, positive Tair was always used to evaluate satellite-derived snowmelt because the occurrence of surface melt corresponds to the spatial pattern of Tair (Tedesco, 2009; Liang et al., 2013). However, melt signals (i.e., the presence of snow liquid water) detected by AMSR-E/2 do not always strictly connect with positive Tair. We have explained the reasons for their differences in **R1C13**.

P5. L32: Accuracy and Kappa should be defined somewhere.

R1C17: The overall accuracy and Kappa coefficient were defined in the revised manuscript:

> The overall accuracy (p_0, the proportion of observed agreement) and Kappa coefficient $k = (p_0 - p_c)/(1 - p_c)$ were used to measure the coincidence based on the confusion matrix, where p_c is the proportion in agreement due to chance (Cohen, 1960).

P6. L9 (Eq 4): This is only true under the assumption that SIC did not change within the_12h from ascending to descending overflight. This should be mentioned. The method could be optimized in this regard by using the Tbs to retrieve the ice concentration in ascending and descending separately and then calculate the DAV with the aid of an open water tie point (which does not cancel out in case SICs are different for ascending and descending overflights)

R1C18: We thank the referee for pointing out this issue.

Yes, the equation is true under the assumption that SIC is the same for both passes. We revised this part to clarify:

Regardless of the atmospheric effects, the Tb of sea ice is comprised of the ice portion (Tb_{ice}) and open water portion (Tb_{ow}) (Markus and Cavalieri, 1998):

$$Tb = Tb_{ice}\ SIC + Tb_{ow}\ (1\text{-}SIC) \quad (3)$$

therefore, $DAV36_{ice}$ can be calculated as follows:

$$DAV36_{ice} = \left| \frac{Tb_{V36A} - Tb_{ow}(1-SIC_A)}{SIC_A} - \frac{Tb_{V36D} - Tb_{ow}(1-SIC_D)}{SIC_D} \right| \quad (4)$$

where SIC_A and SIC_D represent the SIC for ascending and descending passes. If we assume that the SIC of the two passes remains unchanged (i.e., $SIC_A = SIC_D$), then we have:

$$DAV36_{ice} = \frac{|Tb_{V36A} - Tb_{V36D}|}{SIC} \quad (5)$$

We acknowledge the $DAV36_{ice}$ algorithm can be further improved with corresponding SIC for each pass. However, producing a twice-daily SIC product is challenging at present. Extensive simultaneous ground- and space-based observations are needed in the validation. This is likely to be difficult to achieve in polar regions and beyond the scope of this paper. We mentioned this issue in Section 5.2 (Uncertainties):

The DAV36ice algorithm for sea ice snowmelt detection assumes that the SIC of the two passes remains unchanged, which may not be true and lead to misidentifications of melt signals due to quick sea ice drift and disintegration. The algorithm can be further improved if the twice-daily SIC product is available in the future.

P6. L20: accuracy and Kappa definition again

R1C19: Done!

P6. L22: Why is a spatial median needed here, what are erroneous microwave signals?

R1C20: We explained why a spatial median is needed:

Spurious Tb variations may occasionally be mistaken for melt signals, which can be caused by clouds, atmospheric water vapor, wind-induced surface roughening, and residual calibration errors. To mitigate their impacts on melt detection, a median filter with a 3×3 window was applied to the satellite observations.

P6. L25: "Melt freeze-up and duration…." - I don't understand what is meant here

R1C21: Some studies include the analyses of freeze-up (the last day with surface snowmelt) and duration (the days between melt onset and freeze-up) on sea ice (e.g., Markus et al., 2009). However, sufficient Antarctic sea ice melts quickly in austral summer and does not emerge any more in the melting year.

In such cases, the last day with snowmelt is always the day that sea ice disappears, rather than the day that freeze-up begins. We revised this sentence to clarify:

> Sufficient Antarctic sea ice melts quickly in austral summer and does not emerge again in the melting year. In such cases, the last day of snowmelt is always the day that sea ice disappears, rather than the day that freeze-up begins. Thus freeze-up and melt duration were not included in this study.

P6. L29: extend -> extent

R1C22: Done!

P7. L7: if below -5_C means frozen state (P6. L24) and above -1_C means melting, what state is there in between and how is that classified?

R1C23: There is no intermediate state in freeze/thaw cycles. The two conditions were used separately and do not contradict each other:

- The first condition was used to mitigate the effect of spurious Tb variations (see **R1C20**) in melt detection based on AMSR-E/2.
- The second condition was used to derive snowmelt directly based on ERA-Interim Tair.

The first condition was not used to determine the freeze/thaw state. To avoid confusion, we rephrased this sentence:

> Further, melt detection was constrained to the days with compatible thermal regimes following Belchansky et al. (2004). The days with ERA-Interim Tair > -5°C were first determined, and the DAV36 algorithm was applied henceforth.

P7. L16: Discussion about Fig. 5, see also General 2.: the mid July melt onset around -60 to -65 latitude is quite surprising and needs discussion. Also the later melt onset in the more outer parts are interesting. Is it because there was no ice at the melt onset of the more southern regions and ice drifted there later so that melt occurs later in these regions? However, than the MDF should be even higher in these regions, probably close to 100%. I would also suggest not using the parula but a diverging colormap for the difference plot.

R1C24: We thank the referee for pointing out this issue. Yes, this is because sea ice advance (the first day when SIC > 15%) in these areas is later than July 1 (the first day of melting year). Specifically, sea ice does not occur until early September in some parts of the marginal sea ice zone (Stammerjohn et al., 2008) (Fig. R4).

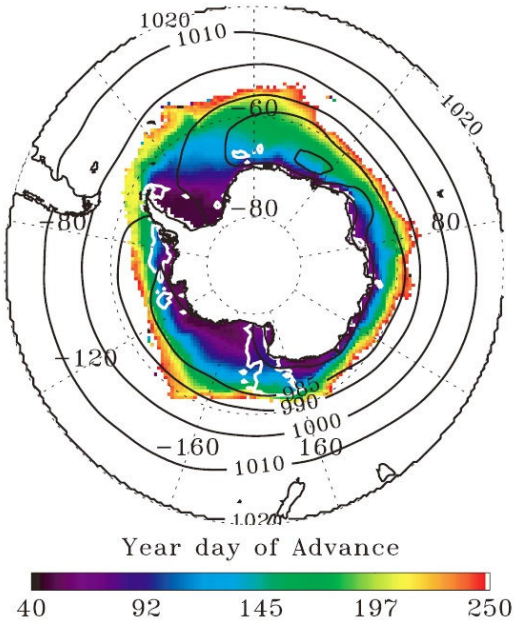

Figure R4. Day of Antarctic sea ice advance over 1979–2004. The figure is adopted from Stammerjohn et al. (2008).

Therefore, early melt onset (EMO) on some marginal sea ice is later than that on the sea ice in lower altitudes where transient melt events can occur before September (e.g., Fig. R1c).

We mentioned this issue in the revised manuscript:

> In some parts of the marginal sea ice zone, EMO was later than that in higher altitudes. This is because sea ice did not occur in these regions until early September (Stammerjohn et al., 2008), while transient surface snowmelt can occur before that in August at lower latitudes (Supplement Fig. 2). However, the earliest CMO was still found in the marginal sea ice zone (Fig. 5b,d).

Fig. 5 was also redrawn as suggested.

P7. L31: “Fig. 5k-o” -> ”Fig. 5g-i”

R1C25: Done.

P8. Discussion about Fig. 6: I would suggest splitting the histograms to maybe a 7 by 3 plot to be able to discuss the particular regions better. Also bin size in the histograms is too small, i.e., the histograms are to noisy to comfortable read their data.

R1C26: Fig. 6 was redrawn as suggested.

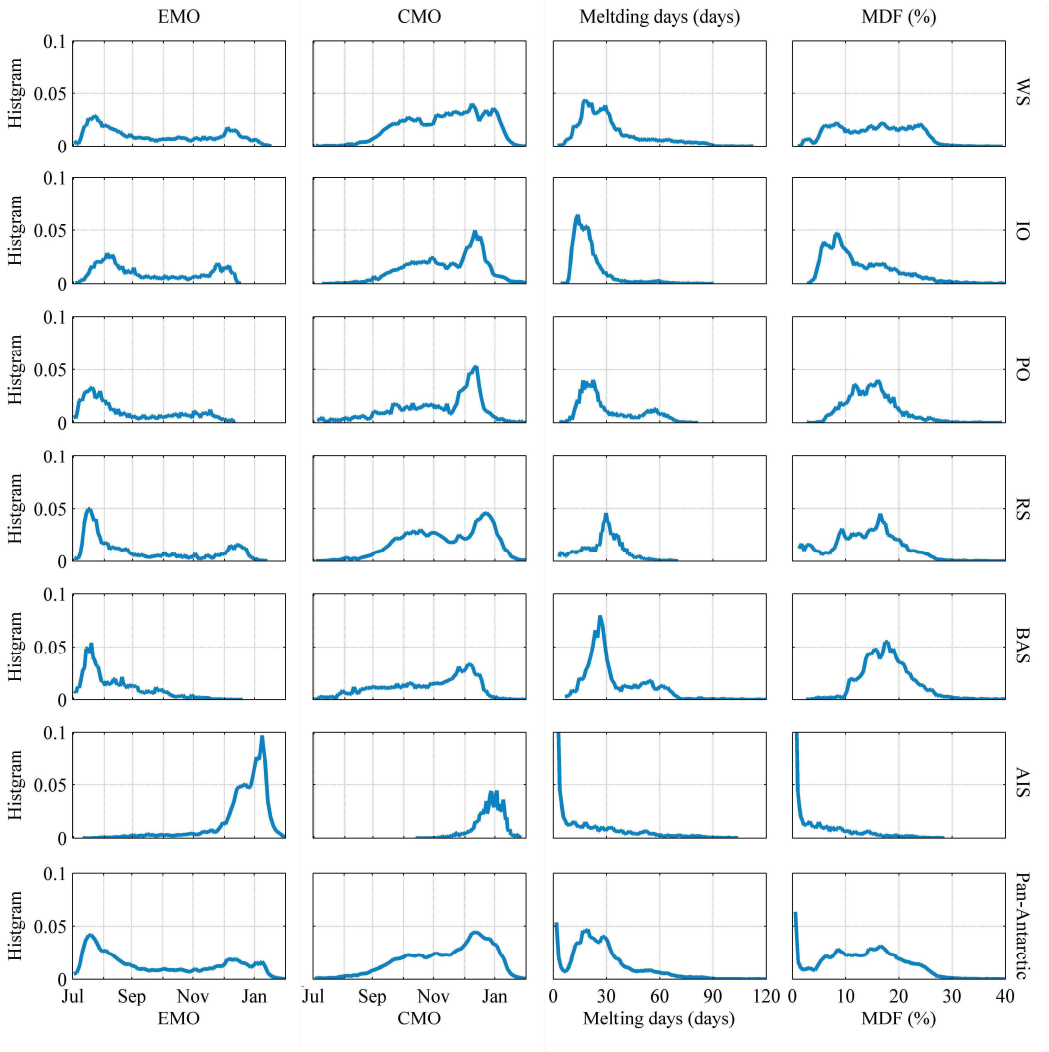

P8. L11-12: The comparison of the melt extent of AIS with the sea ice area makes no sense in my opinion. The AIS is a much smaller region. What is the purpose of this comparison? I suggest to remove Figure 7 completely. However, the melt extentis quite small in the early months like July/August on sea ice which actually contradicts the early melt onset in Fig. 6. This also indicates that the early melt onset is probably just a random noise effect since it does not cover a large area apparently.

R1C27: We thank the referee for pointing out this issue.

- We agree that the comparison between melt extent and sea ice extent makes little contribution to this work. The comparison and Fig.7a were removed, but we would like to keep Fig. 7b which illustrates the seasonal evolution of surface snowmelt. In addition, melt extent fraction (MEF) will

be further discussed in Section 5.3 (Response of the pan-Antarctic surface snowmelt to atmospheric indices).

- The occurrence of early snowmelt onset (EMO) does not result in a significant increase in melt extent because the early melt events are always short-lived. Instead, the histogram of continuous melt onset (CMO) suggests most of the pan-Antarctic continuous snowmelt began between October and January (Fig. 6) when MEF increased quickly (Fig. 7).
- Snowmelt can occur in austral winter on both Antarctic ice sheet (Kuipers Munneke et al., 2018) and the Antarctic sea ice (Massom et al., 2001). In Fig. R1c, winter melt events have been clearly observed based on both AMSR-E and SSM/I measurements, accompanied by positive Tair.

Yes, these early melt events are always short-lived, and can be easily regarded as random noises. We have conducted data preprocessing and quality control to mitigate the effect of spurious Tb variations on melt detection:

Spurious Tb variations may occasionally be mistaken for melt signals, which can be caused by clouds, atmospheric water vapor, wind-induced surface roughening, and residual calibration errors. To mitigate their impacts on melt detection, a median filter with a 3×3 window was applied to the satellite observations. Further, melt detection was constrained to the days with compatible thermal regimes following Belchansky et al. (2004). The days with ERA-Interim Tair > -5°C were first determined, and the DAV36 algorithm was applied henceforth.

P8. L17: with "mean maximum MEF" you mean the "Mean anual Maximum MEF" right? should than be changed in the text.

R1C28: We mean the maximum of daily mean MEF, this part was removed as suggested (see **R1C27**).

P9. L2: I actually do not understand how the trends are calculated. Fig 9 indicates that you calculate the trends pixel based. One would expect that neighbouring pixel having similar melt onset dates (Fig 9a). If the shown pixel based trends have any significance also the spatial pattern should be coherent.

R1C29: Yes, the trends were calculated for each pixel.

- There are a large number of transient melt events during the melt seasons (Fig. 6). Melt onset always shows considerable spatial and temporal variations. A similar phenomenon can be found in the Arctic (Fig. R5) (Stroeve et al., 2014).

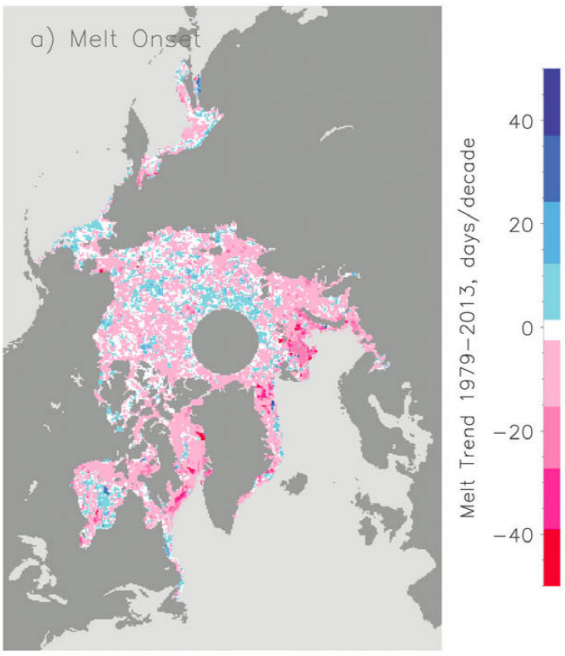

Figure. R5. Trends in Arctic sea ice snowmelt onset from 1979 to 2013. This figure is adopted from Stroeve et al (2014).

- Actually, most of the trends were not statically significant. We redrew Fig.9 with additional significance levels of the trends.

P11. L 18: I suspect the values and discussion to change in case you reconsidered the early snowmelt onset

R1C30: We assume the referee would like to see the analyses and discussion of continuous melt onset (CMO), which were included in the revised manuscript.

Author Response to Referee #2

This study makes use of passive microwave data from AMSRE and AMSR2 to detect melt over the Antarctic Ice Sheet and sea ice regions using a diurnal difference in brightness temperature algorithm. Means and trends in melt onset, number of melt days, and melt day fractions from 2002-2017 are presented and compared with ERA estimates of surface melt based on air temperature, and SSMI melt indices. A method of improving melt detection in marginal sea ice is also presented and validated.

In general the paper is well written and of great interest with excellent figures but a few points need to be addressed. There are many instances where the use (or not) of the definite article is incorrect, I suggest a read through by a native English speaker to correct these.

R2C1: We are sorry for the grammatical problems and the inconvenience they caused in reading. The manuscript was thoroughly revised and edited by a native speaker. We hope it can meet the journal's standards.

Early on it should be made clear that satellite algorithms for melt retrieval detect either the presence or absence of liquid water, or the diurnal transition between the two, rather than actual melting events.

R2C2: Yes, microwave sensors only detect snow liquid water rather than snowmelt. We clarified this issue in the revised manuscript:

> Therefore, snowmelt can be detected via microwave radiometry by identifying the sharp changes in microwave brightness temperatures (Tb) caused by the presence of snow liquid water (Serreze et al., 1993; Liu et al., 2005).

Various products used in this study, Tb, Tair, SIC were undoubtedly supplied at different projections and swaths and resolutions. Please provide more detail on how these products were coregistered.

R2C3: We explained how these products were coregistered:

> The sea ice product is provided in the NSIDC EASE-Grid projection, which is the same as the AMSR-E/2 products. The 0.5° gridded ERA-Interim reanalysis was reprojected to the NSIDC EASE-Grid, and resampled to the same spatial resolution as the passive microwave measurements (25 km).

The validation described briefly P5, L28 does not give enough detail. What is the 'melt signal determined by satellite'? How are the accuracy and coefficients referred to calculated? Why is this agreement 'in contrast'? In contrast to what?

R2C4: Melt signal determined by satellite is actually the presence of snow liquid water. The overall accuracy and Kappa coefficient were clearly defined. "By contrast" was changed to "However". The evaluation method was described in more details to clarify these issues:

> The verification of snowmelt is difficult, especially in the pan-Antarctic where meltwater refreezes quickly, and climatic data are sparse. However, surface snowmelt is determined by atmospheric conditions and agrees well with the Tair distribution pattern (Tedesco, 2007; Liang et al., 2013). In-situ Tair measurements at Zhongshan Station (69.37°S, 76.38°E) obtained from the Chinese National Arctic and Antarctic Data Center (www.chinare.org.cn) were used to evaluate the DAV36 algorithm (Fig. 2). The overall accuracy (p_0, the proportion of observed agreement) and Kappa coefficient $k = (p_0 - p_c)/(1 - p_c)$ were used to measure the coincidence based on the confusion matrix, where p_c is the proportion in agreement due to chance (Cohen, 1960). Tb_{V36A} and Tb_{V36D} showed sharp increases at melt onset, while decreased below the winter mean in the late melt seasons with associated snow metamorphism. However, positive maximum Tair agreed well with melt signals (i.e., the presence of liquid water) determined by the DAV method, with an overall accuracy of 0.93 and a Kappa coefficient of 0.79.

P1, L21. It does not make sense to compare snow melt extents of sea ice and ice sheets when they cover different areas in total. What is the point?

R2C5: We agree that the comparison between melt extent and sea ice extent makes little contribution to this work. The comparison and Fig.7a were removed, but we would like to keep Fig. 7b which illustrates the seasonal evolution of surface snowmelt. In addition, melt extent fraction (MEF) will be further discussed in Section 5.3 (Response of the pan-Antarctic surface snowmelt to atmospheric indices).

P1, L28. You mean snow melt leads to an increase in size of snow grains.

R2C6: Good catch. We rephrased this sentence:

> Intense snowmelt leads to the formation of melt ponds on sea ice and ice sheets, which in turn absorb more radiation and induce further snowmelt through melt-albedo feedback (Tanaka et al., 2016; Bell et al., 2018).

P1, L30. You confuse ice sheets on bedrock, with the hydrofracture on ice shelves which are floating. Separate the discussion of these two impacts.

R2C7: Revised as suggested:

Meltwater may fill in the ice crevasses on ice sheets and migrate to the ice-bedrock surface, which can induce the acceleration of ice flow (Zwally et al., 2002; Sundal et al., 2011). Meltwater can also transport heat into crevasses and deepen them, providing the conditions for ice shelves to break up through hydrofracturing (Scambos et al., 2000; van den Broeke, 2005).

P3, L13. It needs to be made clearer why DAV is more likely to detect melt with AMSRE/2. Ie Explain why time of day (rather than period) of the overpasses is important.

R2C8: The acquisition time is important for melt detection for two reasons:

- First, measurements with stable acquisition time are superior in the analyses of inter-annual snowmelt dynamics. AMSR-E and AMSR2 operate in controlled-orbits measurements, and the crossing time for the two sensors are nearly the same. By contrast, crossing time differs between SSM/I sensors and also changes significantly over the years of operation due to orbit degradation (Picard and Fily, 2006).
- Second, the Antarctic diurnal melt area varies approximately as a sinusoid with the peak in the afternoon and the trough in the early morning (Picard and Fily, 2006). Compared with SSM/I, AMSR-E/2 have more opportunities to detect melt events in the pan-Antarctic due to warmer and colder periods for ascending and descending passes and an expected higher DAV. Taking 2002-2003 as an example, the local acquisition time of ascending and descending SSM/I Tb product south of 40° S were 19.17±0.44 and 5.45±0.45, while they were 14.16±0.20 and 0.88±0.20 for AMSR-E Tb product.

We revised this paragraph to make it clear:

Most of these studies investigated surface snowmelt on sea ice and ice sheets based on SSM/I sensors. However, SSM/I observations show considerable variations in local acquisition time because of orbit degradation (Picard and Fily, 2006). By contrast, the Advanced Microwave Scanning Radiometer for the Earth Observing System (AMSR-E) and the Advanced Microwave Scanning Radiometer 2 (AMSR2) operate in controlled-orbits so that local acquisition time shows little temporal variation (http://www.remss.com/support/crossing-times). AMSR-E/2 measurements with a stable orbit are superior in the analyses of inter-annual snowmelt dynamics. Diurnal melt area in the Antarctic varies approximately as a sinusoid with the peak in the afternoon

and the trough in the early morning (Picard and Fily, 2006). AMSR-E/2 can monitor the Antarctic sea ice and ice sheet (referred to as pan-Antarctic) surface snowmelt at the appropriate local acquisition time. Taking 2002-2003 as an example, the local acquisition time of ascending and descending SSM/I Tb products south of 40° S were 19.17±0.44 and 5.45±0.45, respectively, while these values were 14.16±0.20 and 0.88±0.20 for the AMSR-E Tb products. Compared with SSM/I, AMSR-E/2 have more opportunities to detect melt events in the pan-Antarctic due to warmer and colder periods for ascending and descending passes and an expected higher DAV.

P3, L21. 'Meltwater on the AIS always refreezes instantaneously'. Needs a reference. Also,in this case, it would never be detected.

R2C9: We thank the referee for pointing out the mistake. We mean meltwater can refreezes quasi-instantaneously. We revised this sentence with appropriate citations:

Meltwater on the Antarctic ice sheet (AIS) can refreeze quasi-instantaneously (van den Broeke et al., 2010a) and contributes little to the surface mass balance (The IMBIE team, 2018).

P4, L7. Changes 'almost shares' to 'shares almost'.

R2C10: Done.

P4, L17. This sentence does not make sense. Please rewrite. Which air temperature was used? 2 m?

R2C11: Yes, the 2 m Tair from the gridded ERA-Interim reanalysis was used in this study. We rewrote this paragraph:

ERA-Interim is a global reanalysis produced by the European Centre for Medium-Range Weather Forecasts (ECMWF). The ERA-Interim reanalysis includes various surface parameters, describing weather, ocean and land-surface conditions since 1979 (Dee et al., 2011). The 6-hourly air temperature (Tair) from the gridded ERA-Interim reanalysis at 2 m height was used to assist with melt detection based on AMSR-E/2, as well as directly determine snowmelt in this study.

P4, L29. Please move reference to Fig. 1 to later in this paragraph. You have not yet described the simulations.

R2C12: Done.

P5, L8. Replace ‘opposite’ with ‘contrasting’.

R2C13: Done.

P5, L12. Replace ‘prevailing’ with ‘prevalent’.

R2C14: Done.

P5, L19. Replace ‘extensively’ with ‘extensive’.

R2C15: Done.

P7, L19. This sentence needs rewording ‘MDF decreases in an opposite trend’ suggests that MDF decreases going from high to low latitudes.

R2C16: Good catch. We rewrote this sentence:

> In general, snowmelt shows significant latitudinal zonality. EMO and CMO occur later from the marginal sea ice to the inland of the AIS, from low-latitudes to high-latitudes, while MDF increases in the opposite direction.

P6, L24. How is this definition of frozen based on ERA Tair used in the algorithm?

R2C17: This condition was used to mitigate the effect of spurious Tb variations on melt detection based on AMSR-E/2, rather than determine snowmelt.

To avoid confusion, we rephrased this sentence:

> Further, melt detection was constrained to the days with compatible thermal regimes following Belchansky et al. (2004). The days with ERA-Interim Tair > -5°C were first determined, and the DAV36 algorithm was applied henceforth.

P7, L31. Figs. 5k-o? should be g-i?

R2C18: Corrected.

P8, L12. Again, what is the point of comparing melt extents of sea ice and AIS?

R2C19: We agree that the comparison between melt extent and sea ice extent makes little contribution to this work. We removed this part in the revised manuscript.

P8, L16. It is not clear why the decreasing sea ice extent would lead to an increasing sea ice melt extent? This would only explain the delayed peak in sea ice MEF.

R2C20: We mean the peak of sea ice melt extent does not occur in the warmest period because sea ice considerably declines before January. This part was removed in the revised manuscript.

Fig. 9. You should only plot those pixels with a significant trend. Or also plot the p values.

R2C21: Good suggestion. We added black points in Fig.9 to indicate the pixels with significant trends above the 90% confidence level.

P9, L14. You should discuss further implications of the failure of DAV when melt is continuous. This would presumably manifest as a decrease in Melt Days detected where melt temporal continuity became more prevalent. Might this also explain areas with very early melt onset such as in BAS but a surprisingly low number of melt days.

R2C22: This is an important point. We added the discussion about this issue in Section 5.2 (Uncertainties):

> The regions with snowmelt that became more prevalent would presumably show a decrease in melting days based on the DAV method. Fortunately, unlike the Arctic, surface snowmelt on the Antarctic sea ice is always patchy and relatively short-lived (Drinkwater and Liu, 2000).

Yes, the earliest melt onset was found in BAS, but the highest melting days (37 days) and MDF (17%) were also found in this region. But the melt onset was very early but not too many melt events were detected in RS. We mentioned this point in the revised manuscript:

> The might also be the reason that the melt onset was very early in RS while few melt events were detected by AMSR-E/2.

P10, L25. Please include these correlations between atmospheric indices and melt in a table.

R2C23: We added a table (Table 3) to show the correlations between the atmospheric indices and melt indices.

> Table 3. Correlation between snowmelt index and atmospheric index for the Period 2002–2017.

Correlation coefficients with *, ** and *** indicate statistical significance at 90%, 95%, and 99% confidence levels, respectively.

Atmospheric index	Melt index	WS	IO	PO	RS	BAS	AIS	All
SAM	EMO	-0.27	0.77***	0.32	0.16	0.25	0.52*	0.31
	CMO	-0.03	0.15	0.03	0.50*	0.53*	0.80***	0.54**
	Melting days	0.37	0.18	0.01	-0.26	-0.42	-0.88***	-0.02
	MDF	0.18	-0.11	-0.07	-0.48*	-0.53*	-0.88***	-0.33
SOI	EMO	0.11	-0.08	-0.01	0.10	0.28	0.55**	0.19
	CMO	0.09	-0.23	0.14	-0.53*	-0.12	0.18	-0.31
	Melting days	0.03	-0.26	0.07	-0.11	0.46*	-0.03	-0.07
	MDF	-0.16	-0.18	0.12	0.15	0.34	-0.03	-0.09
Nino3.4	EMO	-0.28	-0.06	-0.11	-0.02	-0.26	-0.47*	-0.27
	CMO	-0.15	0.19	-0.35	0.66**	0.28	0.01	0.35
	Melting days	0.04	0.42	-0.16	0.08	-0.54**	-0.15	-0.07
	MDF	0.24	0.36	-0.11	-0.22	-0.46*	-0.15	0.13

Author Response to Editor

p6L22 "if we assume": what happens if you don't make this assumption. How much do the results change? What impact does this assumption has on the final outcome.

EC1: Open water shows a much lower Tb and may dampen melt signals in marginal sea ice zone. Therefore, we employed $DAV36_{ice}$ (i.e., DAV36 contributed by the ice-covered portion) rather than DAV36 (the difference between AMSR-E/2 ascending and descending 36.5 GHz Tb) in melt detection on sea ice. $DAV36_{ice}$ can be calculated based on the sea ice concentration (SIC) for ascending and descending passes.

- However, no twice-daily SIC product is available now, and the daily SIC product is the best alternative if we assume that the SIC of the two passes remains unchanged.
- $DAV36_{ice}$ can not be solved if we don't make this assumption. We acknowledge this assumption may not be true and lead to misidentifications of melt signals when sea ice drifts or disintegrates quickly, and the $DAV36_{ice}$ algorithm can be further improved with corresponding SIC for each pass. We discussed this issue in the revised manuscript:

  The $DAV36_{ice}$ algorithm for sea ice snowmelt detection assumes that the SIC of the two passes remains unchanged, which may not be true and lead to misidentifications of melt signals due to quick sea ice drift and disintegration. The algorithm can be further improved if the twice-daily SIC product is available in the future.

p9 + table 2: please also add uncertainties (+- x days) on the observed trends and indicate how these uncertainties were calculated. If the uncertainties are in the same order of magnitude as the trends, the trends do not mean much.

EC2: Good suggestion. The uncertainties of the trends were added in the revised manuscript:

Table 2. Trends in pan-Antarctic EMO, CMO, melting days and MDF during 2002-2017. Trends with *, ** and *** indicate statistical significance at 90%, 95%, and 99% confidence levels, respectively. The uncertainties of the trends were estimated at 90% confidence level.

Melt index	WS	IO	PO	RS	BAS	AIS	All
EMO (days yr^{-1})	-0.35±1.10	0.09±0.82	1.37±1.40	1.72±0.71***	2.13±1.88*	0.71±0.76	0.68±0.59*
CMO (days yr^{-1})	-0.82±0.72*	-0.84±0.51**	-0.16±0.71	0.52±1.23	0.59±1.74	0.22±0.51	-0.22±0.43
Melting days (days yr^{-1})	0.34±0.33*	0.37±0.42	0.80±0.46***	-0.52±0.43*	-0.05±0.57	-0.33±0.41	0.11±0.20
MDF (% yr^{-1})	0.20±0.14**	0.15±0.14*	0.19±0.12**	-0.14±0.14	0.02±0.19	-0.09±0.11	0.07±0.08

Other changes in the revised manuscript include:

- We have made mistakes in statistical analyses in the first version, but they do not affect the main conclusion of this study. We corrected these mistakes and checked the manuscript carefully.
- The manuscript was edited by a native English speaker and the grammatical errors were corrected.
- Figure 5-13 was redrawn, two figures were added as supplements.

Recent changes in pan-Antarctic surface snowmelt detected by AMSR-E and AMSR2

Lei Zheng[1], Chunxia Zhou[1], Tingjun Zhang[2], Qi Liang[1], Kang Wang[3]

[1]Chinese Antarctic Center of Surveying and Mapping, Wuhan University, Wuhan 430079, China
[2]Key Laboratory of Western China's Environmental Systems (Ministry of Education), College of Earth and Environmental Sciences, Lanzhou University, Lanzhou 730000, China
[3]Institute of Arctic and Alpine Research, University of Colorado Boulder, Boulder, Colorado, 80309, USA

Correspondence to: Chunxia Zhou (zhoucx@whu.edu.cn) and Tingjun Zhang (tjzhang@lzu.edu.cn)

Abstract. Surface snowmelt in the pan-Antarctic, including the Antarctic ice sheet (AIS)~~sea ice~~ and sea ice~~ice sheet~~, is crucial to the mass and energy balance in polar regions and can serve as an indicator of climate change. Here, w~~W~~e investigated the spatial and temporal variations ~~of~~ in the surface snowmelt over the entire pan-Antarctic ~~as a whole~~ from 2002 to 2017 by using the passive microwave remote sensing data. The stable orbit and appropriate acquisition time of the Advanced Microwave Scanning Radiometer for the Earth Observing System (AMSR-E) and the Advanced Microwave Scanning Radiometer 2 (AMSR2) enable us to take full advantage of the daily brightness temperature (Tb) variations to detect the surface snowmelt ~~events~~. In this study, the difference ~~diurnal amplitude variations of~~between AMSR-E/2 ascending and descending ~~vertically polarized~~ 36.5 GHz Tb in vertical polarization (DAV36~~V~~) ~~were~~ was utilized to map the pan-Antarctic snowmelt because it is unaffected by the snow metamorphism. We ~~validated~~ evaluated the DAV36~~V~~ algorithm~~method~~ against ~~the~~ ground-based measurements and further improved the method over the marginal sea ice zone by excluding the effect of open water. Snowmelt detected by AMSR-E/2 data ~~agreed well with that derived by ERA-Interim reanalysis, and~~was ~~much~~ more extensive and persistent than that detected by the Special Sensor Microwave/Imager (SSM/I) data. On average, pan-Antarctic early snowmelt onset (EMO) occurs in late September, while continuous melt onset (CMO) occurs in mid-November. ~~pan-Antarctic snowmelt began on 19 September, and lasted for 32 days. Annual mean melt extent on the Antarctic ice sheet (AIS) was only 9% of that on the Antarctic sea ice.~~ Overall, ~~the~~ pan-Antarctic surface snowmelt showed a trend (at the 90~~5~~% confidence level) towards later ~~melt onset~~EMO (~~0.70~~0.68 days yr^{-1}) during the 2002-2017 period. Pan-Antarctic CMO was significantly correlated (at the 95% confidence level) with summer Southern Annular Mode (SAM). ~~Surface snowmelt was well correlated with atmospheric indices in some regions. Notably, the decreasing~~ The decreased surface snowmelt on the AIS was very likely linked with the enhanced~~ing~~ summer SAM~~Southern Annular Mode~~.

1 Introduction

Surface snowmelt on sea ice and ice sheets has a great influence on the energy ~~and mass~~ exchange between the snow surface and ~~the~~ atmosphere because wet snow has a lower albedo, and thus absorbs~~ing~~ more incoming solar radiation than dry snow

(Steffen, 1995). Intense sSnowmelt leads to the increase of snow grains and the formation of melt ponds on sea ice and ice sheets, which in turn absorb more radiation and induce further snowmelt through melt-albedo feedback (Tanaka et al., 2016; Bell et al., 2018). (Picard and Fily, 2006; Kuipers Munneke et al., 2012; Tanaka et al., 2016). Meltwater may fill in the ice crevasses on ice sheets and migrate to the ice-bedrock surface, which can provide the conditions for ice shelves to break up (Scambos et al., 2000; van den Broeke, 2005) and induce the acceleration of ice flow (Zwally et al., 2002; Sundal et al., 2011). Meltwater can also transport heat into crevasses and deepen them, providing the conditions for ice shelves to break up through hydrofracturing (Scambos et al., 2000; van den Broeke, 2005). Therefore, the spatial and temporal dynamics of surface snowmelt on sea ice and ice sheets have a direct effect on the mass and energy balances in polar regions (Picard and Fily, 2006; van den Broeke et al., 2009; Stroeve et al., 2014)(Abdalati and Steffen, 1997; Anderson and Drobot, 2001; Drobot and Anderson, 2001b; Belchansky et al., 2004; Picard and Fily, 2006; Markus et al., 2009; Mortin et al., 2012; Luckman et al., 2014). The timing and extent of surface snowmelt are indicators of changes in polar climate (Intergovernmental Panel on Climate Change (IPCC), 2014), and thus potentially have regional and global climate implications.

In-situ observations of snowmelt are sparse over sea ice and ice sheets due to the an unfavorable environment. Remote sensing techniques can provide timely data sets for the monitoring of melt events in polar regions. The dielectric constant of snow is a function of frequency, snow temperature, density, salinity, ice particle, volumetric liquid water content and water shape inclusions (Hallikainen et al., 1986; Proksch et al., 2015). When a snowpack starts begins to melt, the most significant change in the electromagnetic properties is an abrupt increase in the dielectric constant, which increases absorption and reduces the penetration depth of microwaves (Ashcraft and Long, 2006). The radiation characteristics of a wet snow mixture are likely to be dominated by the dispersion behavior of liquid water, even when liquid water is only one percent by volume (Hallikainen et al., 1986). Melt signals, tTherefore, snowmelt can be detected via microwave radiometry by identifying the sharp changes in microwave brightness temperatures (Tb) caused by the presence of snow liquid water (Serreze et al., 1993; Liu et al., 2005; Bliss et al., 2017).

Microwave radiometers can operate in regardless of illumination conditionsall and are insensitive to atmospheric conditions. Most spaceborne passive microwave instruments provide more than two daily passes in polar regions. Various algorithms, including the single- and multi-channel methods, have been used to detect snowmelt based on radiometers. Scanning Multi-channel Microwave Radiometer (SMMR) 18 GHz and 37 GHz Tb, and Special Sensor Microwave/Imager (SSM/I) 19 GHz and 37 GHz Tb have been used to detect surface snowmelt on ice sheets when Tb is above a region-specific or user-defined constant depending on the local snow properties (Ridley, 1993; Zwally and Fiegles, 1994; Mote and Anderson, 1995; Tedesco, 2009). Tb received by satellites is also related to the ground physical temperature, clouds and atmospheric water vapor, which may contaminate melt signals in the Tb time series. Multi-channel methods were developed to minimize these interferences, e.g., using a gradient ratio or a cross-polarized gradient ratio (XGPR) between 19 GHz and 37 GHz to detect surface snowmelt on sea ice and ice sheets (Abdalati and Steffen, 1995; Markus et al., 2009; Liang et al., 2013; Arndt et al., 2016)(Steffen et al., 1993; Abdalati and Steffen, 1995; Drobot and Anderson, 2001; Belchansky et al., 2004; Fettweis et al., 2007; Markus et al., 2009; Liang et al., 2013). Snowmelt can also be recognized by usingbased on

edge detection or wavelet transform-based technologies ~~due to~~by identifying the abrupt changes in Tb values ~~for the transitions in freeze-thaw cycles~~ (Joshi et al., 2001; Liu et al., 2005).

Snow grain size increases after the ~~refreezing of snow~~ liquid water refreezes. As a result, dry snow Tb decreases during the melt season due to the increase ~~of~~ in volume scattering (Markus et al., 2009). Therefore, single-channel methods may fail to identify melt events because of the metamorphic snow structures. Ramage and Isacks (2002, 2003) introduced the SSM/I diurnal amplitude variations (DAV, i.e., the Tb difference between ascending and descending passes) ~~of~~in vertically polarized 37 GHz Tb to investigate the snowmelt timing on the Southeast Alaskan Icefields. The DAV method~~algorithm~~ is unaffected by ~~the~~ snow metamorphism in melt detection. This technique has been successfully applied to ~~the~~ ice sheets and was proven~~d~~ to be more sensitive to snow liquid water than the XGPR method (Tedesco, 2007; Zheng et al., 2018). Freeze-thaw cycles on the Antarctic sea ice were also successfully detected based on the SSM/I 37 GHz DAV (Willmes et al., 2009)~~(Willmes et al., 2006, 2009)~~. ~~F~~urthermore, Arndt et al. (2016) distinguished temporary snowmelt from continuous snowmelt on the Antarctic sea ice by combining DAV ~~and~~ with the cross-polarized ratio of SSM/I Tb. In these studies, surface snowmelt patterns ~~have not been~~were not described over the marginal sea ice zone, where the earliest sea ice retreat ~~has been~~was identified ~~based on the passive microwave sea ice concentration (SIC) measurements~~ (Stammerjohn et al., 2008). DAV may not be ~~not~~ strong enough to be identified as melt signals when open water with low Tb emerges in the first-year sea ice zone.

Most of these studies investigated surface snowmelt on sea ice and ice sheets based on SSM/I sensors. However, ~~the~~ SSM/I observations show~~ed~~ considerable variations in local acquisition time because of ~~the~~ orbit degradation (Picard and Fily, 2006). By contrast, the Advanced Microwave Scanning Radiometer for the Earth Observing System (AMSR-E) and the Advanced Microwave Scanning Radiometer 2 (AMSR2) operate~~s~~ in controlled-orbits so that local acquisition time shows little temporal variation (http://www.remss.com/support/crossing-times). AMSR-E/2 measurements with a stable orbit are superior in the analyses of inter-annual snowmelt dynamics. Diurnal melt area in the Antarctic varies approximately as a sinusoid with the peak in the afternoon and the trough in the early morning (Picard and Fily, 2006). ~~In addition,~~ AMSR-E/2 can monitor the Antarctic sea ice and ice sheet (referred to as pan-Antarctic) surface snowmelt at the ~~more~~ appropriate local acquisition time ~~(Zheng et al., 2018)~~. Taking 2002-2003 as an example, the local acquisition time of ascending and descending SSM/I Tb products south of 40° S were 19.17±0.44 and 5.45±0.45, respectively, while these~~y~~ values were 14.16±0.20 and 0.88±0.20 for the AMSR-E Tb products. Compared with SSM/I, AMSR-E/2 have more opportunities to detect melt events in the pan-Antarctic due to ~~a~~ warmer and ~~a~~ colder periods for ascending and descending passes and an expected higher DAV.

Unlike the Arctic sea ice and Greenland ice sheet, ~~the~~ pan-Antarctic surface snowmelt is relatively short-lived and patchy (Drinkwater and Liu, 2000; Picard et al., 2007), and has received much less attention. Contrary to the reduction in sea ice extent, thickness and duration in the Arctic, the Antarctic sea ice presented increasing trends in both extent and duration, especially in the Ross Sea (Comiso and Nishio, 2008; Hobbs et al., 2016). Most of the Antarctic sea ice is snow-covered, even in summer when snowmelt occurs (Brandt et al., 2005). Melt ponds are not often observed on the Antarctic sea ice (Ackley et al., 2008). Meltwater on the Antarctic ice sheet (AIS) ~~always~~ can refreeze~~s~~ quasi-instantaneously (van den Broeke et al., 2010a) and contributes little to the surface mass balance (The IMBIE team, 2018). ~~T~~Although more than 25% of the AIS has

experienced snowmelt since the 1980s, only 2% melts every year (Picard et al., 2007). Melt extent has been decreasing over the AIS since 1987 (Tedesco et al., 2007).

Strong interactions have been found between ~~the~~ sea ice and ice sheet ~~melting conditions~~surface snowmelt through atmospheric circulation (Stroeve et al., 2017). Surface snowmelt dynamics in the West Antarctic and Antarctic peninsula have been found to be related with the sea ice variations in adjacent seas (Scott et al., 2018; Zheng et al., 2019). Previous studies ~~always~~ have separately investigated surface snowmelt on sea ice and ice sheet ~~separately~~, which may result in uncertainties in the integrated study. The DAV method has been successfully applied in snowmelt detection on both sea ice (Willmes et al., 2009) and ice sheet (Tedesco, 2007; Zheng et al., 2018). It is worthwhile to estimate snowmelt over the pan-Antarctic based on a uniform approach. The overall objective of this study is to improve the understanding of surface snowmelt over the pan-Antarctic based on the DAV method in three aspects: (1) to detect the pan-Antarctic surface snowmelt at the stable and appropriate local acquisition time based on AMSR-E/2, (2) to improve the performance of the DAV method~~algorithm~~ in the marginal sea ice zone by excluding the effect of open water, and (3) to estimate the pan-Antarctic surface snowmelt as a whole~~,~~ and systematically describe the surface snowmelt patterns and changes from 2002 to 2017.

2 Data sets

2.1 Data from AMSR-E/2

A~~s a~~ modified version of the AMSR radiometer, the AMSR-E radiometer, launched aboard the NASA Earth Observing System (EOS) Aqua satellite on 4 May 2002. We obtained the 25 km AMSR-E/Aqua L2A global swath spatially-resampled 36 GHz Tb data from the National Snow and Ice Data Center (NSIDC, www.nsidc.org) (Knowles et al., 2006). AMSR2 aboard the Global Change Observation Mission-Water (GCOM-W1) satellite was launched on 18 May 2012 after AMSR-E ceased operations. As a successor of AMSR-E, AMSR2 ~~almost~~ shares almost the same satellite orbit and sensor parameters as AMSR-E, and provides~~ing~~ continuous measurements for the study of global climate change, energy balance and ecosystems. The 25 km AMSR2 Tb ~~at a spatial resolution of 25 km~~ used in this study was provided by the Japan Aerospace Exploration Agency (JAXA, http://suzaku.eorc.jaxa.jp/GCOM/). AMSR-E/2 obtained data over a 1450 km swath. The brightness temperature products~~Tb~~ at 36.5 GHz in vertical polarization (Tb_{V36}) was used to estimate the pan-Antarctic snowmelt extent and timing in this study.

2.2 Sea ice and atmospheric products

The Bootstrap sea ice concentration (SIC) product was used to mask ~~the~~ sea ice in this study (Comiso, 2017). The 25 km daily SIC South Hemisphere product ~~in the south hemisphere with a spatial resolution of 25 km~~ was obtained from the NSIDC (http://nsidc.org/data/nsidc-0079), University of Colorado Boulder. ~~A sea ice pixel was determined when SIC is above 15% (Meier and Stroeve, 2008), and only the pixels with SIC above 80% for at least 5 days were considered in melt detection~~ Pixels

with SIC greater than 80% for less than 5 days were marked as being ice-free (Markus et al., 2009). For a sea ice pixel, SIC above 15% indicates the presence of sea ice (Meier and Stroeve, 2008).

ERA-Interim is a global reanalysis ~~is a sequential data based on the atmospheric model and assimilation system, which~~ produced by the European Centre for Medium-Range Weather Forecasts (ECMWF). ~~Advancing forward in time using 12-hourly analysis cycles, t~~The ERA-Interim reanalysis includes various surface parameters, describing weather, ocean and land-surface conditions since 1979 (Dee et al., 2011). The 6-hourly air temperature (Tair) ~~of~~ from the gridded ERA-Interim reanalysis at 2 m height was used to assist with melt detection based on AMSR-E/2, as well as ~~derive~~ directly determine snowmelt ~~directly~~ in this study.

The sea ice product is provided in the NSIDC EASE-Grid projection, which is the same as the AMSR-E/2 products. The 0.5° gridded ERA-Interim reanalysis was reprojected to the NSIDC EASE-Grid, and resampled to the same spatial resolution as the passive microwave measurements (25 km).

3 Methodology

3.1 Tb and liquid water content

According to the Rayleigh-Jeans approximation, Tb is a function of emissivity (ε) and the near-surface physical temperature (Ts) of snow and ice (Zwally, 1977):

$$Tb = \varepsilon Ts \quad (1)$$

Previous studies have ~~always~~ emphasized the process that Tb increases when the snowpack starts to melt due to the increase ~~of~~ in emissivity. However, Tb decreases after reaching a peak when the volume liquid water is approximately about one percent (Kang et al., 2014). ~~The processes can clearly be seen in the simulations (Fig. 1).~~ We investigated the variations in Tb_{V36} with increasing snow liquid water based on the Microwave Emission Model of Multi-layered Snowpack (MEMLS) (Wiesmann and Mätzler, 1999). In the simulations, snow temperature, density and depth in a homogeneous snowpack were set to 273.15 K, 350 kg m^{-3}, and 20 cm, respectively, by referring to Brucker et al. (2010) and Kang et al. (2014). Snow-ice reflectivity at 36.5 GHz was set to 0.045 in vertical polarization according to Powell et al. (2006). The evolution of Tb with increasing liquid water can be divided into energy saturation and energy dampening phases ~~(Kang et al., 2014)~~. The initial increases in~~of~~ Tb are accompanied by the amplification of ε until the liquid water reaches a certain level. The subsequent energy dampening phase is characterized by monotonic~~ally~~ decreases in~~of~~ Tb, which are caused by the increase in~~of~~ snow-air interface reflectivity due to the amplified real part of the refractive index (Kang et al., 2014) (Fig. 1).

Tb_{V36} of the fine-grained snowpack increases rapidly in the energy saturation phase with a slight amount of liquid water, ~~Daily~~ and daily Tb variations ~~for slight snowmelt~~ are large because of the contrasting ~~opposite~~ freeze/thaw state. Therefore, both single-channel and DAV methods can recognize these sharp changes in the early melt season. During the melt seasons, snow grain size can increase to 2 mm when meltwater refreezes in the pore space (Winebrenner et al., 1994). As a result, Tb_{V36}

of the coarse-grained snowpack is much lower than that of the fine-grained snowpack due to enhanced volume scattering. ~~,~~ Single-channel methods may fail to work when the Tb_{V36} of a melting snowpack is even lower than the winter mean in the late melt season (Zheng et al., 2018). ~~resulting in a much lower Tb in dry snow regime (Markus et al., 2009) (Fig. 2).~~ ~~Consequently~~By contrast, significant daily Tb_{V36} variations ~~also~~ still exist in the transition from a dry to wet snow regime during the heavy melt season, even when day-time Tb_{V36} is in the energy dampening phase (Fig. 1). Diurnal freeze-thaw cycles are ~~in snowpack are~~ prevalent ~~prevailing~~ in polar regions (Hall et al., 2009; Willmes et al., 2009; van den Broeke et al., 2010b)~~,~~ ~~especially for the melt onset with daytime snowmelt and overnight meltwater refreezing~~. The simulations suggest that the DAV method can detect melt signals for both the melt onset (e.g., Willmes et al., 2009) and the entire melt season when diurnal freeze/thaw transition occurs (e.g., Zheng et al., 2018). ~~Single-channel thresholding methods may miss the melt events when Tb decreases due to the associated snow metamorphism, while DAV algorithm can recognize melt signals through the melt season.~~ Moreover, the optimum acquisition time of AMSR-E/2 enables us to take full advantage of the DAV method~~algorithm~~ in melt detection.

3.2 Melt detection methods

A ~~V~~vertically polarized SSM/I 37 GHz DAV (DAV37) has been used in melt detection on the Greenland ice sheet and ~~the~~ Antarctic sea ice (Willmes et al., 2006, 2009; Tedesco, 2007; Arndt et al., 2016). Extensive~~ly~~ summer daily freeze-thaw cycles on the Antarctic sea-ice were found by SSM/I (Willmes et al., 2009). AMSR-E/2 have more opportunities to identify these transitions due to the more appropriate local acquisition time. AMSR-E/2 36.5 GHz DAV in vertical polarization (DAV36), were used to detect the pan-Antarctic snowmelt and calculated as follows:

$$DAV36 = | Tb_{V36A} - Tb_{V36D} | \quad (2)$$

where Tb_{V36A} and Tb_{V36D} are the Tb_{V36} in ~~the~~ ascending and descending passes respectively. Willmes et al. (2009) determined melt signals when the DAV37 of SSM/I ~~37 GHz Tb~~ exceeds 10 K. The threshold ~~has been~~was validated ~~through~~ against extensive field data on the Antarctic sea ice. We utilized the same threshold for melt detection based on AMSR-E/2 DAV36 considering ~~a very close channel.~~ the differences between AMSR-E 36 GHz Tb and SSM/I 37 GHz Tb are very small (Dai and Che, 2010). In the region south of 85° S where the surface snow is stable and never melts, the bias between the two measurements was only approximately 1 K during 2002-2003 (Supplement Fig. 1). Slight Tb offsets between different sensors should not affect the results when using temporal Tb variability in melt detection (Markus et al., 2009).

This method was also applied in the investigation of snow surface freeze/thaw cycles on the AIS. The verification of snowmelt is difficult, especially in the pan-Antarctic where meltwater refreezes quickly, and climatic data are sparse. However, surface snowmelt is determined by atmospheric conditions and agrees well with the Tair distribution pattern (Tedesco, 2007; Liang et al., 2013). In-situ Tair measurements at Zhongshan Station (69.37°S, 76.38°E) obtained from the Chinese National ~~Climatic~~ Arctic and Antarctic Data Center (~~NCDC,~~ www.chinare.org.cn) were used to ~~validate~~ evaluate the DAV36 algorithm (Fig. 2). The overall accuracy (p_0, the proportion of observed agreement) and Kappa coefficient $k = (p_0 - p_c)/(1 - p_c)$ were used

to measure the coincidence based on the confusion matrix, where p_c is the proportion in agreement due to chance (Cohen, 1960). Tb_{V36A} and Tb_{V36D} showed sharp increases at melt onset, while decreased below the winter mean in the late~~during~~ melt seasons with associated snow metamorphism. However, ~~By contrast,~~ positive maximum Tair agreed well with melt signals (i.e., the presence of liquid water) determined by ~~satellites~~the DAV method, with an overall accuracy of 0.93 and a Kappa coefficient of 0.79.

When a snowpack on sea ice ~~starts~~ begins to melt, it appears as a blackbody at microwave wavelengths and the Tb increases sharply (Markus et al., 2009), while open water exhibits ~~relatively~~ much lower Tb (Markus and Cavalieri, 1998). ~~So~~ Therefore, Tb amplitudes may not be ~~not~~ strong enough to be identified as melt signals for ~~the~~ first-year sea ice with sufficient~~plenty of~~ open water. To eliminate the effect of open water in melt detection, $DAV36_{ice}$ (i.e., DAV36 contributed by the ice-covered portion) was applied in the Antarctic sea ice snowmelt detection. Regardless of the atmospheric effects, the Tb of sea ice is comprised ~~by~~ of the ice portion (Tb_{ice}) and open water portion (Tb_{ow}) (Markus and Cavalieri, 1998):

$$Tb = Tb_{ice}\ SIC + Tb_{ow}\ (1\text{-}SIC) \quad (3)$$

therefore, $DAV36_{ice}$ can be calculated as follows:

$$DAV36_{ice} = \left| \frac{Tb_{V36A} - Tb_{ow}(1-SIC_A)}{SIC_A} - \frac{Tb_{V36D} - Tb_{ow}(1-SIC_D)}{SIC_D} \right| \quad (4)$$

where SIC_A and SIC_D represent the SIC for ascending and descending passes. If we assume that the SIC of the two passes remains unchanged (i.e., $SIC_A = SIC_D$), then we have:

$$DAV36_{ice} = \frac{|Tb_{V36A} - Tb_{V36D}|}{SIC} \quad (5)$$

Fig. 3 shows the comparison of meteorological observations of a sea ice buoy in the Weddell Sea and the corresponding AMSR2 measurements. Snow buoy observations (Fig. 3a), including snow depth and Tair, were obtained from the Alfred Wegener Institute (AWI, http://www.meereisportal.de/en/seaicemonitoring/buoy-mapsdata/). The inse~~r~~t map in Fig. 3b illustrates the annual mean SIC and the route of the buoy from multi-year ice to first-year ice in the Weddell Sea. Tb_{V36A} and Tb_{V36D} showed great differences in the melt season. Sporadic melt events were detected before December 2014. Accompanied by a slight decrease of snow depth, DAV36 exceeded 10 K and Tair went above the freezing point after mid-December. $DAV36_{ice}$ was ~~almost~~ nearly equal to DAV36 when SIC was above 90%, while it was much higher than the latter when the SIC dropped after February. DAV36 was below 10 K with Tair above the freezing point ~~for~~ many times (see the black arrows), while these melt signals were successfully recognized by $DAV36_{ice}$ algorithm. The overall accuracy and Kappa coefficient between the positive maximum Tair and ~~the~~ melt signals derived by satellites were 0.79 and 0.51 based on the DAV36 algorithm~~,~~ and ~~were~~ 0.82 and 0.60 based on the $DAV36_{ice}$ algorithm. $DAV36_{ice}$ algorithm performs better than DAV36 algorithm in the marginal ice zone by reducing the effect of open water.

~~In order t~~To capture complete melt seasons, a melting year ~~start~~begins on 1 July and ends on 30 June of the next year. The missing observations were filled based on time-line interpolation. Spurious Tb variations may occasionally be mistaken for

melt signals, which can be caused by clouds, atmospheric water vapor, wind-induced surface roughening, and residual calibration errors. ~~In order to~~ To mitigate their impacts on melt detection~~eliminate erroneous microwave signals~~, a median filter with a 3×3 window ~~of 3×3~~ was applied to the satellite observations. Further, melt detection was constrained to the days with compatible thermal regimes following Belchansky et al. (2004). The days with ERA-Interim Tair > -5°C were first determined, and the DAV36 algorithm was applied henceforth.~~surface snow on sea ice and ice sheet is supposed to be frozen when the daily maximum of ERA-interim Tair is below -5°C.~~ ~~Snowmelt indices~~

Considering the existence of both transient and persistent snowmelt in the pan-Antarctic, early melt onset (EMO, the first day when snowmelt is detected) and continuous melt onset (CMO, the first day when snowmelt lasts for at least three consecutive days) were investigated in this study. ~~including melt onset (first day of snowmelt), and melting days were calculated~~ Melting days was calculated by summing the number of days with snowmelt. ~~based on the above method. Melt freeze-up and duration were not included in this study because plenty of~~ Sufficient Antarctic sea ice melts quickly in austral summer and does not emerge ~~any more~~again in the melting year. In such cases, the last day of snowmelt is always the day that sea ice disappears, rather than the day that freeze-up begins. Thus freeze-up and melt duration were not included in this study. Antarctic sea ice cover has exhibited considerable regional and annual variations (Hobbs et al., 2016). To be consistent, the melting days fraction (MDF) and melt extent fraction (MEF) ~~was~~ were introduced to study the snowmelt variations:

$$\mathrm{MDF}=\frac{\text{Melting days}}{\text{Ice cover days}}, \tag{6}$$

$$\mathrm{MEF}=\frac{\text{Melt extent}}{\text{Ice cover extent}} \tag{~~5~~7}$$

where ice cover was determined with SIC > 15% for sea ice, and the AIS is assumed to be ice-covered all the year.

Melt signals derived from the DAV method and the positive Tair from AWS were not always strictly connected (Figs. 3&4). Their differences may be attributed to inconsistent temporal resolutions because snowmelt and refreezing can occur at any time of the day. The daily maximum Tair was derived from hourly Tair records, while only two daily satellite observations were used in the DAV method. In addition, snowmelt may occur when Tair is below the freezing point because of the penetration and absorption of solar radiation within the snowpack (Koh and Jordan, 1995).~~The verification of snowmelt is difficult, especially in the pan-Antarctic where meltwater refreezes quickly and climatic data are sparse. Nonetheless, surface snowmelt is determined by the atmospheric conditions and agrees well with the Tair distribution pattern (Tedesco, 2007; Liang et al., 2013). Once Tair approaches or exceeds the freezing point, meltwater emerges in the snow packs (Willmes et al., 2006). Owing to the solar radiation penetration and absorption within the snow pack, subsurface snow temperature can be higher than the surface on the AIS (Brandt and Warren, 1993), and snowmelt may occur when Tair is below the freezing point (Koh and Jordan, 1995; Zhang et al., 1996, 2001). Arctic sea ice freeze/thaw states were successfully determined when Tair is above -1°C (Markus et al., 2009).~~ Markus et al. (2009) have determined the Arctic sea ice freeze/thaw states based on gridded Tair data set with a threshold of -1°C. To evaluate the performance of the DAV method on a larger scale~~In this study~~, snowmelt

over the pan-Antarctic was also determined by ERA-interim reanalysis when the daily maximum Tair ~~goes above~~exceeded -1°C. ~~The ERA-derived snowmelt was used to compare with satellite observations.~~

4 Results

4.1 Snowmelt distribution

The study area was divided into six parts to investigate regional discrepanc~~y~~ies in~~of~~ surface snowmelt on sea ice and ice sheet according to Parkinson and Cavalieri (2012) (Fig. 4), namely, the Weddell Sea (WS, 60 °W to 20 °E), Indian Ocean (IO, 20 °E to 90 °), Pacific Ocean (PO, 90 °E to 160 °E), Ross Sea (RS, 160 °E to 130 °W), Bellingshausen Amundsen Sea (BAS, 130 °W to 60 °W), and the AIS.

Integrated pan-Antarctic annual ~~snowmelt~~ melt indices ~~was~~ were ~~generated~~ examined based on AMSR-E/2 (Fig. 5a-~~c~~d). On average, pan-Antarctic EMO occurred on 24 September (DOY 86), CMO arrived 53 days later (16 November)~~snowmelt began on 19 September (DOY 81)~~, and snowmelt lasted for 30~~2~~ days during 2012-2017 (Table 1). In general, snowmelt shows significant~~ly~~ latitudinal zonality. ~~Melt onset~~EMO and CMO occur ~~came~~ later from the marginal sea ice to the inland of the AIS, from low-latitudes to high-latitudes, while MDF increases in the opposite direction~~decreased in an opposite trend (Fig. 5a-c)~~. In some parts of the marginal sea ice zone, EMO was later than that in higher altitudes. This is because sea ice did not occur in these regions until early September (Stammerjohn et al., 2008), while transient surface snowmelt can occur before that in August at lower latitudes (Supplement Fig. 2). However, the earliest CMO was still found in the marginal sea ice zone (Fig. 5b,d).

__ Annual mean ~~melt onset~~EMO, CMO, melting days and MDF of the six regions were also analyzed (Table 1). In terms of the satellite observations, the earliest ~~snowmelt~~ EMO (15 August) and CMO (5 November) occurred in BAS where surface snow melted for 37 days.~~melt seasons began on 10 August (DOY 41) and melted for 40 days.~~ As expected, snowmelt on the AIS began the latest with EMO occurring on 7 December and CMO occurring on 18 December. ~~Snowmelt on the AIS, as expected, began the lateston 4 December (DOY 158) and lasted for only 26 days on average. Surface snow of the multi-year sea ice in WS and BAS~~ Sea ice surface snow in WS can melt for more than 100 days (Fig. 5c~~b~~). MDF can reach 30% for the marginal sea ice in~~of~~ RS and WS (Fig. 5d~~e~~). Snowmelt at high-latitudes was variable. For example, surface snowmelt on the Ross Ice Shelf extended to the inland area and even reached the Transantarctic Mountains in 2004-2005, but ~~it~~ the Ross Ice Shelf was almost totally frozen during 2009-2011 (not shown).

The spatial distribution patterns of pan-Antarctic surface snowmelt derived from AMSR-E/2 and ERA generally agreed well with each other, especially for the AIS (Table 1 and Fig. 5). On average, pan-Antarctic EMO and CMO derived by satellites were 12 days and 27 days later than that detected by ERA. AMSR-E/2 detected later EMO on the near-shore sea ice, and later CMO in BAS and RS (Fig. 5i,j). ~~Snowmelt onset derived by AMSR-E/2 and ERA agreed well with each other (Table 1 and Fig. 5), especially for the marginal sea ice. On average, melt onset derived by satellites was 6 days earlier than that detected by ERA. Local discrepancies existed in the near-shore sea ice where ERA detected earlier snowmelt onset (Fig. g).~~

ERA recognized more melt events in WS (16 2days), BAS (19 6days), and RS (20 17days), where intense surface snowmelt was found (Fig. 5kh). Satellite-based MDF for the marginal sea ice is lower than that derived by ERA (Fig. 5li). With the exception of the Antarctic Peninsula where the melt season can last for more than three months, the AIS melt timings detected by the two methods were consistent with each other (Fig. 5i-l5k-o).

Seasonal evolution of snowmelt in different regions was examined by the normalized histograms of annual mean melt onsetEMO, CMO, melting days and MDF (Fig. 6). Notable differences existed between the temporal distribution of sea ice and ice sheet melt patterns., which can be seen in the two peaks for the pan-Antarctic melt onset histograms (Fig. 6a). Sea ice melt onsetEMO concentrated in mid-July for BAS, and in early August for IO. By contrast, the frequency of AIS melt onset EMO did not reach the peak until early January (Fig. 6a). The occurrence of pan-Antarctic CMO peaked in December, varying from early December in BAS and WS to late December in the AIS. Melting days and MDF histograms indicate a large number of transient melt events, especially in the AIS.Pan-Antarctic annual mean melting days and MDF were32 days and 14% respectively (Table 1), while melting days histogram indicates a large number of transient snowmelt with only a few melt events, especially for the AIS (Fig. 6b). About 30 Approximately16% of the AIS experienced snowmelt over 2002-2017;, however, approximately 66% of these areasabout 67% of the AIS melt area melted for no more than 5 days. In general, melting days seldom exceeded 45 d, with the exception of the BAS and WS where plenty of surface snow can melt for more than two months. The annual mean MDF in the BAS was 1726% (Table 1), while the MDF in most of the AIS kept was below 5% (Fig. 6e).

Daily melt extent on the Antarctic sea ice and AIS was calculated and presented in Fig. 7a. Annual mean melt extent on the AIS (0.18×10^6 km^2) was only 9% of that on the Antarctic sea ice (1.92×10^6 km^2). The AIS was almost totally frozen in winter (JJA) when plenty of first-year ice still melted. Sea ice extent decreased in October accompanied by the increasing sea ice melt extent. AIS melt extent began to extend about two months later. Sea ice melt extent reached the peak in mid-December with a mean maximum of 7.01×10^6 km^2, while the peak of AIS melt extent appeared in mid-January with a mean maximum of 1.15×10^6 km^2. Sea ice melt extent peaked earlier due to the simultaneous decreasing sea ice extent.

The CMO histogram suggests that most of the pan-Antarctic continuous snowmelt began between October and January (Fig. 6), corresponding to a sharp increase in MEF (Fig. 7). In mid-January, most of the Antarctic sea ice experienced surface snowmelt, and the daily mean MEF can reach 80%.with a mean maximum MEF of 84%. The AIS daily mean MEF was much lower, and also reached the a maximum (8%) in mid-January (Fig. 7b). MEF declined rapidly between late January and March. The Antarctic sea ice daily mean MEF declined to below 10% and the AIS became almost completely refrozen after April.

4.2 Trend analysis

Trends in surface melting conditions during 2002-2017 were analyzed. Linear trends in the melt indices were calculated based on the annual departures. As listed in Table 2, the pan-Antarctic snowmelt as a wholeoverall showed a significant trend (at the 905% confidence level) towards later melt onsetEMO (0.7 0.68 days yr^{-1}), especially in the RS, and BAS and PO. Trends in CMO, melting days and MDF were not statistically significant for the pan-Antarctic. Melt onsetEMO came significantly later

(at the 99% confidence level) in ~~the~~ RS (~~1.65~~1.72 days yr^{-1}). M~~eanwhile, m~~elting days ~~and MDF~~ in RS was also significantly decreased (at the 90~~95~~% confidence level). The largest trend in ~~melt onset~~EMO (2.13 days yr^{-1}) was observed in BAS. CMO occurred significantly earlier in WS and IO where MDF also significantly increased. Melting days and MDF have both significantly increased (above the 95% confidence level) in PO. ~~Though melt onset in PO came significantly later (at 95% confidence level) with a rate of 1.44 days yr^{-1}, melting days and MDF have both increased in this period. The changes in melt indices in WS and IO were small and not significant.~~ The AIS showed a negative trend in surface snowmelt with a later ~~melt onset (0.79 days yr^{-1})~~EMO and CMO, and slightly decreasing melting days and MDF.

The inter-annual departures of melt indices for the pan-Antarctic, AIS and RS where the most significant change in EMO was found are shown in Fig. 8. Melt indices showed considerable inter-annual variations. Pan-Antarctic EMO came much later in recent years after reaching the earliest point in 2010-2011. ~~The inter-annual departures of melt onset, melting days and MDF are presented for the pan-Antarctic, the AIS and the RS where the most significant changes in melting conditions were found (Fig. 8). Although the 2010-2011 season showed the earliest melt onset, and largest MDF, the maximum annual mean melting days were found in the 2009-2010 season. Consistent with the pan-Antarctic,~~ RS and AIS presented negative trends in surface snowmelt, which were indicated by all the melt indices. The earliest ~~melt onset~~EMO in RS ~~were~~ was found in 2004-2005 when ~~almost~~ nearly the entire Ross Ice Shelf ~~also~~ experienced snowmelt. All the AIS snowmelt indices indicated the weakest melt season in 2014-2015.

The considerable decrease ~~of~~ in surface snowmelt in the RS can also be clearly seen in Fig. 9, which illustrates the trends in ~~the~~ melt indices during 2002-2017. Most of the pan-Antarctic showed a later ~~melt onset~~EMO, especially in RS ~~and BAS~~ where melting days ~~and MDF~~ also presented remarkable negative trends. Surface snow on the East Antarctic sea ice, especially in PO, ~~also~~ presented trends towards a later ~~melt onset~~EMO. ~~;~~ ~~h~~However, melting days and MDF in these regions have increased. ~~Surface snowmelt onset~~EMO and CMO appeared earlier on the marginal sea ice in WS where melting days and MDF also significantly increased. Many low-lying ice shelves in the AIS, such as the Larsen C Ice Shelf in the Antarctic Peninsula and the Abbot Ice Shelf in Marie Byrd Land, presented trends towards decreasing melting days and MDF.

5 Discussion

5.1 Comparisons

EMO and CMO derived from ERA were earlier than that detected by AMSR-E/2 data ~~ERA detected earlier melt than AMSR-E/2 data~~ (Fig. 5 and Table 1). This is because it takes time to produce liquid water when snow temperature approaches the melting point (Markus et al., 2009). Daily Tb variation is limited when liquid water does not refreeze or snowpack is still melting in the warm nights during heavy melt seasons (Willmes et al., 2009; Semmens and Ramage, 2014). As a result, ERA recognized more melt events for the regions where heavy snowmelt was found and the DAV ~~algorithm~~ method fails to work, such as the WS, BAS, RS and the Larsen C ice shelf. The might also be the reason that the melt onset was very early in RS while few melt events were detected by AMSR-E/2.

Willmes et al. (2009) established the SSM/I DAV ~~algorithm~~ method to study the Antarctic sea ice ~~surface snowmelt~~CMO (hereafter W09). Antarctic sea ice CMO mapped by AMSR-E shows a higher spatial continuity than that in W09. CMO derived from the two satellites agreed well with each other at high latitudes during 2002-2008. However, W09 found a remarkably later CMO on the marginal sea ice compared with results from AMSR-E (Fig. 10). ~~A remarkably later snowmelt onsetwas detected by W09 during 2002-2008 when compared with results derived from AMSR-E and ERA data in this study, especially for the marginal sea ice (Fig. 10).~~ There are several reasons for the significant difference in marginal sea ice CMO detected by ~~snowmelt detection on sea ice by using~~ AMSR-E and SSM/I data. First, W09 only studied surface snowmelt on sea ice after 1 October, while the melt season begins on 1 July in this study., ~~we started from 1 July to 30 June in the next year. Second, daily Tb variations contributed by snowmelt on sea ice portion were extracted by the DAV36$_{ice}$ algorithm (Eq. 4), snowmelt signals were amplified by reducing the effect of open water~~ Second, the DAV36$_{ice}$ algorithm can amplify snowmelt signals by reducing the effect of open water, so that more melt events can be recognized (Fig. 3). Third, compared with SSM/I, AMSR-E operated in a stable orbit and observed the pan-Antarctic with more appropriate local acquisition time, and hence had more opportunities to identify melt events (Supplement Fig. 2).

Considering that snowmelt can be biased by various SMMR and SSM/I acquisition times, Picard and Fily (2006) retrieved the AIS surface snowmelt ~~of the AIS~~ based on corrected 18-19 GHz Tb time series (hereafter PF06). The AIS daily melt extent derived by AMSR-E/2 and ERA were consistent ~~well~~ with each other with R^2=0.923. The PF06 daily melt extent also presented a high correlation with results from AMSR-E/2 (R^2=0.778). However, the melt extent derived by PF06 was significantly smaller than that mapped by AMSR-E/2 (Fig. 11a). AMSR-E/2 and ERA daily mean melt extent were more than twice the melt extent mapped by PF06 from December to February (Fig. 11b). During the melt seasons, Tb may decrease due to the strong volume scattering resulting~~ed~~ from the snow metamorphism (Ramage and Isacks, 2002; Markus et al., 2009). Summer Tb can even be ~~even~~ much lower than the winter observations (Zheng et al., 2018)~~(see in Fig. 2)~~. PF06 determined snowmelt when the SSM/I 19 GHz Tb exceeds the winter mean plus 2.5 times ~~of~~ the standard deviation of the winter Tb;~~,~~ therefore, it may underestimate surface snowmelt. Moreover, as explained in Section 3.1 and as shown in Fig. 1, Tb decreases during~~in~~ the energy dampening phase ~~during heavy snowmelt~~. Single-channel methods such as~~like~~ PF06 may miss the melt signals during a heavy melt season, while the DAV method~~algorithm~~ is unaffected by ~~the~~ snow metamorphism and can detect snowmelt even during~~in~~ the energy dampening phase.

5.2 Uncertainties

There are several uncertainties in the pan-Antarctic snowmelt derived from~~by~~ AMSR-E/2 data. First, the DAV method~~algorithm~~ may fail to work when liquid water does not refreeze or snowpack is still melting in warm nights (Willmes et al., 2009~~; Semmens and Ramage, 2014~~). The regions with snowmelt that became more prevalent would presumably show a decrease in melting days based on the DAV method. Fortunately, unlike the Arctic, surface snowmelt on the Antarctic sea ice is always patchy and relatively short-lived (Drinkwater and Liu, 2000). Second, although the DAV ~~algorithm~~ method used in this study performs well when compared with ~~ERA-interim reanalysis and~~ meteorological observations, the optimal threshold

may differ temporally and regionally with varying snow properties. In addition, ice disintegrates, brine and flooding effects may play an important role in seasonal and even diurnal sea ice Tb variations, further complicating the story (Smith, 1998; Willmes et al., 2009). Arndt et al. (2016) utilized individual local thresholds with a median value of 6 K to detect snowmelt based on SSM/I DAV and recognized an earlier melt onset than W09. Melt indices derived ~~by~~ from the DAV ~~algorithm~~ method showed considerable variations when applying different thresholds (from 6 to 14 K in Fig. 12). Varying the threshold applied to AMSR-E/2 DAV by ±4 K results in -17~~12~~ days to 14~~9~~ days departure for the annual mean ~~melt onset~~EMO, and -9~~6~~ days to 12~~8~~ days departure for annual mean melting days. It should be noted that the presence of snow liquid water detected by AMSR-E/2~~It is worth noticing that liquid water~~ does not necessarily mean that the~~a~~ snowpack is melting because it takes time for meltwater to refreeze ~~(van den Broeke et al., 2010b)~~. In addition, after ~~the~~ refreezing of surface snow, subsurface liquid water can still be detected by radiometer due to the penetrating capacity of microwaves (Ashcraft and Long, 2006~~; Picard et al., 2007; Wang et al., 2016~~). The DAV36$_{ice}$ algorithm for sea ice snowmelt detection assumes that the SIC of the two passes remains unchanged, which may not be true and lead to misidentifications of melt signals due to quick sea ice drift and disintegration. The algorithm can be further improved if the twice-daily SIC product is available in the future.

5.3 Response of the pan-Antarctic surface snowmelt to atmospheric indices

Snowmelt in the pan-Antarctic was found to be strongly associated with the atmospheric component of the El-Niño Southern Oscillation (ENSO) and the Southern Annular Mode (SAM) (Turner, 2004; Tedesco and Monaghan, 2009; Oza et al., 2011; Meredith et al., 2017). In January 2016, the extensive surface snowmelt in ~~west~~ West Antarctica was likely linked with sustained and strong advection of warm marine air due to the concurrent strong El Nino event (Nicolas et al., 2017). The weakly negative trend in~~of~~ surface temperature in Antarctica was consistent with the positive trends in ~~the~~ SAM during summer and autumn since the 1970s (Monaghan et al., 2008).

To study the response of the pan-Antarctic surface snowmelt to atmospheric conditions, we explored the relationship between the melt indices and ~~the~~ Nino3.4 (Rayner et al., 2003), Southern Oscillation Index (SOI) (Ropelewski et al., 1987) and SAM (Marshall, 2003) (Table 3). The CMO of the pan-Antarctic was significantly correlated (at the 95% confidence level) with summer (DJF) SAM. CMO and MDF were also well correlated with summer SAM in RS, BAS and AIS. The correlation coefficient between EMO and SAM was the highest (0.77) in IO. ~~No statistically significant correlations were found between these synoptic variables and the entire pan-Antarctic snowmelt. However, surface snowmelt was well correlated with these indices in some regions. An Anti-correlation was found between summer (DJF) SOI and MDF (R= 0.50, p<0.1)~~ CMO was significantly correlated with SOI and Nino3.4 in RS. Melting days and MDF were also found to be strongly correlated with summer SOI or Nino3.4 in BAS where strong decreases in sea-ice concentration and duration were always linked with contemporary ENSO warm events (Kwok et al., 2002; Bromwich et al., 2004~~; Matear et al., 2015~~).

MDF was negatively related to summer SAM for off-shore sea ice in BAS and RS where MDF has significantly decreased (Fig. 13~~a~~)~~,~~ ~~t~~This relationship was especially significant in the AIS (R=-0.88, P<0.01). High anti-correlations were found between summer SAM and the annual mean MEF on the Antarctic sea ice and AIS (Fig. 13b). The significantly decreased~~ing~~

(at the 95% confidence level) annual mean melt extent on the AIS (-0.37×10^4 km^2 yr^{-1}) during 2002-2017 was strongly associated with increasing summer SAM (R=-0.82, P<0.0~~0~~1). This phenomenon is in line with the decreased~~ing~~ surface snowmelt and the enhanced~~ing~~ summer SAM in AIS since the 1970s (Marshall, 2003; Tedesco and Monaghan, 2009). ~~Though AIS melt onset was also well correlated with Nino3.4 (R=0.63, P<0.05), SAM was the principal driver of AIS near-surface temperature and snowmelt variability (Marshall, 2007; Tedesco and Monaghan, 2009).~~ The positive SAM results in anomalously strong westerlies over the Southern Ocean and hence the reduction in poleward heat transport, leading to the~~a~~ subsequent atmospheric cooling in the Antarctic regions (Thompson and Solomon, 2002). SAM is the principal driver of AIS near-surface temperature and snowmelt variability (Marshall, 2007; Tedesco and Monaghan, 2009), and it is expected to have a continuous effect on the Antarctic climate in the next few decades considering the projected ozone recovery (Thompson et al., 2011). ~~The SAM is expected to have a continuous effect on the Antarctic climate and surface melting conditions in the next decades considering the projected ozone recovery (Thompson et al., 2011).~~

6 Conclusions

In this study, we investigated the pan-Antarctic surface melting conditions during 2012-2017~~, including melt onset, melting days, MDF and MEF,~~ by using daily AMSR-E/2 Tb variations. Compared with SSM/I, the more stable orbit and more appropriate local acquisition time of AMSR-E/2 enable us to take full advantage of the DAV method ~~algorithm~~ to investigate surface melt events. The performance of this method~~the DAV algorithm~~ was improved in the marginal sea ice zone by excluding the effect of open water. ~~T~~Although the DAV method~~algorithm~~ may fail to recognize melt events when meltwater does not refreeze or snowpack ~~even~~ melts in the warm nights, snowmelt detected by AMSR-E/2 agreed well with ~~that derived by ERA-interim reanalysis~~the positive Tair observations, and was more extensive than that detected by SSM/I.

Pan-Antarctic snowmelt showed significant~~ly~~ latitudinal zonality. On average, early snowmelt begins in late September, while continuous snowmelt begins in mid-November.~~the pan-Antarctic snowmelt began on 19 September (DOY 81).~~ Sea ice in WS ~~and BAS~~ can melt for more than 100 days. Snowmelt on the Antarctic sea ice and ~~ice sheet~~AIS exhibited great differences in temporal distribution patterns. ~~Annual mean melt extent on the AIS was only 9% of that on the Antarctic sea ice.~~ The pan-Antarctic showed a significant trend (at the 90~~5~~% confidence level) towards later EMO (0.68 days yr^{-1})~~melt onset (0.7 days yr^{-1})~~. Negative trends in snowmelt were found in RS~~, BAS,~~ and AIS. CMO in the pan-Antarctic was well correlated with summer SAM. The decreasing surface snowmelt in the AIS was very likely linked with the positive summer SAM trend during 2002-2017.

Though AMSR-E/2 observed the pan-Antarctic at the appropriate time for ~~the~~ snowmelt detection, they may underestimate snowmelt because snowmelt can occur at any time and ~~the~~ refreezing ~~is~~ can be quasi-instantaneous. Other sources of the microwave remote sensing data set, such as scatterometer and synthetic aperture radar, are expected to enrich daily ~~the daily~~

pan-Antarctic snowmelt observations in future works. Snowmelt derived by satellites can serve as input and , as well as output validations for climate models.

Data availability

The AMSR-E and AMSR2 data were obtained from the National Snow and Ice Data Center (NSIDC) and the Japan Aerospace Exploration Agency (JAXA). Sea ice concentration data was also provided by NSIDC. The ERA-Interim is available from the European Centre for Medium-Range Weather Forecasts (ECMWF).

Competing interests

The authors declare that they have no conflict of interest.

Acknowledgements

The authors would like to thank the National Snow and Ice Data Center (NSIDC) and the Japan Aerospace Exploration Agency (JAXA) for providing AMSR-E and AMSR2 data respectively. Sea ice concentration data was also obtained from NSIDC. European Centre for Medium-Range Weather Forecasts (ECMWF) is thanked for providing the ERA-interim reanalysis.

We would like to express our gratitude to the editor and reviewers for their careful and insightful comments. The numerical calculations in this paper have been done on the supercomputing system in the Supercomputing Center of Wuhan University. This research was funded by the National Natural Science Foundation of China (NSFC) (Grant nos. 41376187, 41531069 and 41776200).

References

Abdalati, W. and Steffen, K.: Passive microwave-derived snow melt regions on the Greenland Ice Sheet, Geophys. Res. Lett., 22(7), 787–790, doi:10.1029/95GL00433, 1995.

Ackley, S. F., Lewis, M. J., Fritsen, C. H. and Xie, H.: Internal melting in Antarctic sea ice: Development of "gap layers," Geophys. Res. Lett., 35, L11503, doi:10.1029/2008GL033644, 2008.

Arndt, S., Willmes, S., Dierking, W. and Nicolaus, M.: Timing and regional patterns of snowmelt on Antarctic sea ice from passive microwave satellite observations, J. Geophys. Res. Ocean., 121(8), 5916–5930, doi:10.1002/2015JC011504, 2016.

Ashcraft, I. S. and Long, D. G.: Comparison of methods for melt detection over Greenland using active and passive microwave measurements, Int. J. Remote Sens., 27(12), 2469–2488, doi:10.1080/01431160500534465, 2006.

Belchansky, G. I., Douglas, D. C. and Platonov, N. G.: Duration of the Arctic sea ice melt season: Regional and interannual variability, 1979-2001, J. Clim., 17(1), 67–80, doi:10.1175/1520-0442(2004)017<0067:DOTASI>2.0.CO;2, 2004.

Bell, R. E., Banwell, A. F., Trusel, L. D. and Kingslake, J.: Antarctic surface hydrology and impacts on ice-sheet mass balance, Nat. Clim. Chang., 8(12), 1044–1052, doi:10.1038/s41558-018-0326-3, 2018.

Bliss, A., Miller, J. and Meier, W.: Comparison of Passive Microwave-Derived Early Melt Onset Records on Arctic Sea Ice, Remote Sens., 9(3), 199, doi:10.3390/rs9030199, 2017.

Brandt, R. E., Warren, S. G., Worby, A. P. and Grenfell, T. C.: Surface albedo of the Antarctic sea ice zone, J. Clim., 18(17), 3606–3622, doi:10.1175/JCLI3489.1, 2005.

Bromwich, D. H., Monaghan, A. J. and Guo, Z.: Modeling the ENSO modulation of Antarctic climate in the late 1990s with the Polar MM5, J. Clim., 17(1), 109–132, doi:10.1175/1520-0442(2004)017<0109:MTEMOA>2.0.CO;2, 2004.

Brucker, L., Picard, G. and Fily, M.: Snow grain-size profiles deduced from microwave snow emissivities in Antarctica, J. Glaciol., 56(197), 514–526, doi:10.3189/002214310792447806, 2010.

Cohen, J.: A Coefficient of Agreement for Nominal Scales, Educ. Psychol. Meas., 20(1), 37–46, doi:10.1177/001316446002000104, 1960.

Comiso, J.: Bootstrap Sea Ice Concentrations from Nimbus-7 SMMR and DMSP SSM/I-SSMIS, Version 3. NASA National Snow and Ice Data Center Distributed Active Archive Center, NSIDC, doi:10.5067/7Q8HCCWS4I0R, 2017.

Comiso, J. C. and Nishio, F.: Trends in the sea ice cover using enhanced and compatible AMSR-E, SSM/I, and SMMR data, J. Geophys. Res., 113, C02S07, doi:10.1029/2007JC004257, 2008.

Dai, L. and Che, T.: Cross-platform calibration of SMMR, SSM/I and AMSR-E passive microwave brightness temperature, Sixth Int. Symp. Digit. Earth Data Process. Appl., 7841, 784103, doi:10.1117/12.873150, 2010.

Dee, D. P., Uppala, S. M., Simmons, A. J., Berrisford, P., Poli, P., Kobayashi, S., Andrae, U., Balmaseda, M. A., Balsamo, G., Bauer, P., Bechtold, P., Beljaars, A. C. M., van de Berg, L., Bidlot, J., Bormann, N., Delsol, C., Dragani, R., Fuentes, M., Geer, A. J., Haimberger, L., Healy, S. B., Hersbach, H., Hólm, E. V., Isaksen, L., Kållberg, P., Köhler, M., Matricardi, M., McNally, A. P., Monge-Sanz, B. M., Morcrette, J.-J., Park, B.-K., Peubey, C., de Rosnay, P., Tavolato, C., Thépaut, J.-N. and Vitart, F.: The ERA-Interim reanalysis: configuration and performance of the data assimilation system, Q. J. R. Meteorol. Soc., 137(656), 553–597, doi:10.1002/qj.828, 2011.

Drinkwater, M. R. and Liu, X.: Seasonal to interannual variability in Antarctic sea-ice surface melt, IEEE Trans. Geosci. Remote Sens., 38(4), 1827–1842, doi:10.1109/36.851767, 2000.

Hall, D. K., Nghiem, S. V., Schaaf, C. B., DiGirolamo, N. E. and Neumann, G.: Evaluation of surface and near-surface melt characteristics on the Greenland ice sheet using MODIS and QuikSCAT data, J. Geophys. Res. Earth Surf., 114, F04006, doi:10.1029/2009JF001287, 2009.

Hobbs, W. R., Massom, R., Stammerjohn, S., Reid, P., Williams, G. and Meier, W.: A review of recent changes in Southern Ocean sea ice, their drivers and forcings, Glob. Planet. Change, 143, 228–250, doi:10.1016/J.GLOPLACHA.2016.06.008, 2016.

Intergovernmental Panel on Climate Change (IPCC): Climate change 2013: the physical science basis. Fifth assessment report of the intergovernmental panel on climate change, 2014.

Joshi, M., Merry, C. J., Jezek, K. C. and Bolzan, J. F.: An edge detection technique to estimate melt duration, season and melt extent on the Greenland Ice Sheet using Passive Microwave Data, Geophys. Res. Lett., 28(18), 3497–3500, doi:10.1029/2000gl012503, 2001.

Kang, D. H., Barros, A. P. and Dery, S. J.: Evaluating Passive Microwave Radiometry for the Dynamical Transition From Dry to Wet Snowpacks, IEEE Trans. Geosci. Remote Sens., 52(1), 3–15, 2014.

Knowles, M., Armstrong, R. and Brodzik, M. J.: AMSR-E/Aqua Daily EASE-Grid Brightness Temperatures, Version 1. Boulder, Colorado USA. NASA National Snow and Ice Data Center Distributed Active Archive Center, NSIDC, doi:https://doi.org/10.5067/RRR4WWORG070, 2006.

Koh, G. and Jordan, R.: Sub-surface melting in a seasonal snow cover, J. Glaciol., 41(139), 474–482, doi:10.3189/S002214300003481X, 1995.

Kwok, R., Comiso, J. C., Kwok, R. and Comiso, J. C.: Southern Ocean Climate and Sea Ice Anomalies Associated with the Southern Oscillation, J. Clim., 15(5), 487–501, doi:10.1175/1520-0442(2002)015<0487:SOCASI>2.0.CO;2, 2002.

Liang, L., Guo, H., Li, X. and Cheng, X.: Automated ice-sheet snowmelt detection using microwave radiometer measurements, Polar Res., 32(1), 1–13, doi:10.3402/polar.v32i0.19746, 2013.

Liu, H., Wang, L. and Jezek, K. C.: Wavelet-transform based edge detection approach to derivation of snowmelt onset, end and duration from satellite passive microwave measurements, Int. J. Remote Sens., 26(21), 4639–4660, doi:10.1080/01431160500213342, 2005.

Markus, T. and Cavalieri, D. J.: Snow Depth Distribution Over Sea Ice in the Southern Ocean from Satellite Passive Microwave Data, in Antarctic Sea Ice: Physical Processes, Interactions and Variability, vol. 74, pp. 19–39., 1998.

Markus, T., Stroeve, J. C. and Miller, J.: Recent changes in Arctic sea ice melt onset, freezeup, and melt season length, J. Geophys. Res. Ocean., 114, C12024, doi:10.1029/2009JC005436, 2009.

Marshall, G. J.: Trends in the Southern Annular Mode from observations and reanalyses, J. Clim., 16(24), 4134–4143, doi:10.1175/1520-0442(2003)016<4134:TITSAM>2.0.CO;2, 2003.

Marshall, G. J.: Half-century seasonal relationships between the Southern Annular Mode and Antarctic temperatures, Int. J. Climatol., 27(3), 373–383, doi:10.1002/joc.1407, 2007.

Matear, R. J., O'Kane, T. J., Risbey, J. S. and Chamberlain, M.: Sources of heterogeneous variability and trends in Antarctic sea-ice, Nat. Commun., 6, 8656, doi:10.1038/ncomms9656, 2015.

Meier, W. N. and Stroeve, J.: Comparison of sea-ice extent and ice-edge location estimates from passive microwave and enhanced-resolution scatterometer data, Ann. Glaciol., 48, 65–70, doi:10.3189/172756408784700743, 2008.

Meredith, M. P., Stammerjohn, S. E., Venables, H. J., Ducklow, H. W., Martinson, D. G., Iannuzzi, R. A., Leng, M. J., van Wessem, J. M., Reijmer, C. H. and Barrand, N. E.: Changing distributions of sea ice melt and meteoric water west of the Antarctic Peninsula, Deep Sea Res. Part 2. Top. Stud. Oceanogr., 139, 40–57, doi:10.1016/j.dsr2.2016.04.019, 2017.

Monaghan, A. J., Bromwich, D. H., Chapman, W. and Comiso, J. C.: Recent variability and trends of Antarctic near-surface temperature, J. Geophys. Res. Atmos., 113, D04105, doi:10.1029/2007JD009094, 2008.

Mote, T. L. and Anderson, M. R.: Variations in snowpack melt on the Greenland ice sheet based on passive-microwave measurements, J. Glaciol., 41(137), 51–60, 1995.

Nicolas, J. P., Vogelmann, A. M., Scott, R. C., Wilson, A. B., Cadeddu, M. P., Bromwich, D. H., Verlinde, J., Lubin, D., Russell, L. M., Jenkinson, C., Powers, H. H., Ryczek, M., Stone, G. and Wille, J. D.: January 2016 extensive summer melt in West Antarctica favoured by strong El Niño, Nat. Commun., 8, 15799, doi:10.1038/ncomms15799, 2017.

Oza, S. R., Singh, R. K. K., Vyas, N. K. and Sarkar, A.: Study of inter-annual variations in surface melting over Amery Ice Shelf, East Antarctica, using space-borne scatterometer data, J. Earth Syst. Sci., 120(2), 329–336, 2011.

Parkinson, C. L. and Cavalieri, D. J.: Antarctic sea ice variability and trends, 1979–2010, Cryosph., 6, 871–880, doi:10.5194/tc-6-871-2012, 2012.

Picard, G. and Fily, M.: Surface melting observations in Antarctica by microwave radiometers: Correcting 26-year time series from changes in acquisition hours, Remote Sens. Environ., 104(3), 325–336, 2006.

Picard, G., Fily, M. and Gallee, H.: Surface melting derived from microwave radiometers: A climatic indicator in Antarctica, Ann. Glaciol., 46, 29–34, doi:10.3189/172756407782871684, 2007.

Powell, D. C., Markus, T., Cavalieri, D. J. and Gasiewski, A. J.: Microwave Signatures of Snow on Sea Ice: Modeling, IEEE Trans. Geosci. Remote Sens., 44(11), 3091–3102, 2006.

Ramage, J. M. and Isacks, B. L.: Determination of melt-onset and refreeze timing on southeast Alaskan icefields using SSM/I diurnal amplitude variations, Ann. Glaciol., 34, 391–398, doi:10.3189/172756402781817761, 2002.

Ramage, J. M. and Isacks, B. L.: Interannual variations of snowmelt and refreeze timing on southeast-Alaskan icefields, U.S.A., J. Glaciol., 49(164), 102–116, doi:10.3189/172756503781830908, 2003.

Rayner, N. A., Parker, D. E., Horton, E. B., Folland, C. K., Alexander, L. V., Rowell, D. P., Kent, E. C. and Kaplan, A.: Global analyses of sea surface temperature, sea ice, and night marine air temperature since the late nineteenth century, J. Geophys. Res., 108(D14), 4407, doi:10.1029/2002JD002670, 2003.

Ridley, J.: Surface melting on Antarctic Peninsula ice shelves detected by passive microwave sensors, Geophys. Res. Lett., 20(23), 2639–2642, doi:10.1029/93GL02611, 1993.

Ropelewski, C. F., Jones, P. D., Ropelewski, C. F. and Jones, P. D.: An Extension of the Tahiti–Darwin Southern Oscillation Index, Mon. Weather Rev., 115(9), 2161–2165, doi:10.1175/1520-0493(1987)115<2161:AEOTTS>2.0.CO;2, 1987.

Scambos, T., Hulbe, C., Fahnestock, M. and Bohlander, J.: The link between climate warning and break-up of ice shelves in the Antarctic Peninsula, J. Glaciol., 46(154), 516–530, doi:10.3189/172756500781833043, 2000.

Scott, R. C., Nicolas, J. P., Bromwich, D. H., Norris, J. R. and Lubin, D.: Meteorological Drivers and Large-Scale Climate Forcing of West Antarctic Surface Melt, J. Clim., 32(3), 665–684, doi:10.1175/JCLI-D-18-0233.1, 2018.

Semmens, K. and Ramage, J.: Melt patterns and dynamics in Alaska and Patagonia derived from passive microwave brightness temperatures., Remote Sens., 6(1), 603–620, doi:10.3390/rs6010603, 2014.

Serreze, M. G., Maslanik, J. A., Scharfen, G. R., Barry, R. G. and Robinson, D. A.: Interannual variations in snow melt over Arctic sea ice and relationships to atmospheric forcings, Ann. Glaciol., 17, 327–331, doi:10.3189/S0260305500013057, 1993.

Smith, D. M.: Observation of perennial Arctic sea ice melt and freeze-up using passive microwave data, J. Geophys. Res. Ocean., 103(C12), 27753–27769, doi:10.1029/98JC02416, 1998.

Stammerjohn, S. E., Martinson, D. G., Smith, R. C., Yuan, X. and Rind, D.: Trends in Antarctic annual sea ice retreat and advance and their relation to El Niño–Southern Oscillation and Southern Annular Mode variability, J. Geophys. Res., 113, C03S90, doi:10.1029/2007JC004269, 2008.

Steffen, K.: Surface energy exchange at the equilibrium line on the Greenland ice sheet during onset of melt, Ann. Glaciol., 21, 13–18, 1995.

Stroeve, J. C., Markus, T., Boisvert, L., Miller, J. and Barrett, A.: Changes in Arctic melt season and implifications for sea ice loss, Geophys. Res. Lett., 41, 1216–1225, doi:10.1002/2013GL058951.Received, 2014.

Stroeve, J. C., Mioduszewski, J. R., Rennermalm, A., Boisvert, L. N., Tedesco, M. and Robinson, D.: Investigating the Local Scale Influence of Sea Ice on Greenland Surface Melt, Cryosph., 11, 2363–2381, doi:10.5194/tc-2017-65, 2017.

Sundal, A. V., Shepherd, A., Nienow, P., Hanna, E., Palmer, S. and Huybrechts, P.: Melt-induced speed-up of Greenland ice sheet offset by efficient subglacial drainage, Nature, 469(7331), 521–524, doi:10.1038/nature09740, 2011.

Tanaka, Y., Tateyama, K., Kameda, T. and Hutchings, J. K.: Estimation of melt pond fraction over high-concentration Arctic sea ice using AMSR-E passive microwave data, J. Geophys. Res. Ocean., 121(9), 7056–7072, doi:10.1002/2016JC011876, 2016.

Tedesco, M.: Snowmelt detection over the Greenland ice sheet from SSM/I brightness temperature daily variations, Geophys. Res. Lett., 34, L02504, doi:10.1029/2006GL028466, 2007.

Tedesco, M.: Assessment and development of snowmelt retrieval algorithms over Antarctica from K-band spaceborne brightness temperature (1979-2008), Remote Sens. Environ., 113(5), 979–997, doi:10.1016/j.rse.2009.01.009, 2009.

Tedesco, M. and Monaghan, A. J.: An updated Antarctic melt record through 2009 and its linkages to high-latitude and tropical climate variability, Geophys. Res. Lett., 36, L18502, doi:10.1029/2009GL039186, 2009.

Tedesco, M., Abdalati, W. and Zwally, H. J.: Persistent surface snowmelt over Antarctica (1987–2006) from 19.35 GHz brightness temperatures, Geophys. Res. Lett., 34, L18504, doi:10.1029/2007gl031199, 2007.

The IMBIE team: Mass balance of the Antarctic Ice Sheet from 1992 to 2017, Nature, 558(7709), 219–222, doi:10.1038/s41586-018-0179-y, 2018.

Thompson, D. W. J. and Solomon, S.: Interpretation of recent Southern Hemisphere climate change, Science, 296(5569), 895–899, doi:10.1126/science.1069270, 2002.

Thompson, D. W. J., Solomon, S., Kushner, P. J., England, M. H., Grise, K. M. and Karoly, D. J.: Signatures of the Antarctic ozone hole in Southern Hemisphere surface climate change, Nat. Geosci., 4(11), 741–749, doi:10.1038/ngeo1296, 2011.

Turner, J.: The El Niño-Southern Oscillation and Antarctica, Int. J. Climatol., 24(1), 1–31, doi:10.1002/joc.965, 2004.

van den Broeke, M.: Strong surface melting preceded collapse of Antarctic Peninsula ice shelf, Geophys. Res. Lett., 32, L12815, doi:10.1029/2005GL023247, 2005.

van den Broeke, M., Bamber, J., Ettema, J., Rignot, E., Schrama, E., van de Berg, W., van Meijgaard, E., Velicogna, I. and Bert, W.: Partitioning recent Greenland mass loss, Science, 326(5955), 984–986, doi:10.1126/science.1178176, 2009.

van den Broeke, M., König-Langlo, G., Picard, G., Kuipers Munneke, P. and Lenaerts, J.: Surface energy balance, melt and sublimation at Neumayer Station, East Antarctica, Antarct. Sci., 22(1), 87–96, doi:10.1017/S0954102009990538, 2010a.

van den Broeke, M., Bus, C., Ettema, J. and Smeets, P.: Temperature thresholds for degree-day modelling of Greenland ice sheet melt rates, Geophys. Res. Lett., 37, L18501, doi:10.1029/2010GL044123, 2010b.

Wang, L., Toose, P., Brown, R. and Derksen, C.: Frequency and distribution of winter melt events from passive microwave satellite data in the pan-Arctic, Cryosph., 10, 2589–2602, doi:10.5194/tc-10-2589-2016, 2016.

Wiesmann, A. and Mätzler, C.: Microwave emission model of layered snowpacks, Remote Sens. Environ., 70(3), 307–316, doi:10.1016/S0034-4257(99)00046-2, 1999.

Willmes, S., Bareiss, J., Haas, C. and Nicolaus, M.: The importance of diurnal processes for the Seasonal cycle of Sea-ice microwave brightness temperatures during early Summer in the Weddell Sea, Antarctica, Ann. Glaciol., 44, 297–302, doi:10.3189/172756406781811817, 2006.

Willmes, S., Haas, C., Nicolaus, M. and Bareiss, J.: Satellite microwave observations of the interannual variability of snowmelt on sea ice in the Southern Ocean, J. Geophys. Res., 114, C03006, doi:10.1029/2008JC004919, 2009.

Winebrenner, D. P., Nelson, E. D., Colony, R. and West, R. D.: Observation of melt onset on multiyear Arctic sea ice using the ERS 1 synthetic aperture radar, J. Geophys. Res., 99(C11), 22425–22441, doi:10.1029/94JC01268, 1994.

Zheng, L., Zhou, C., Liu, R. and Sun, Q.: Antarctic Snowmelt Detected by Diurnal Variations of AMSR-E Brightness Temperature, Remote Sens., 10(9), 1391, doi:10.3390/rs10091391, 2018.

Zheng, L., Zhou, C. and Liang, Q.: Variations in Antarctic Peninsula snow liquid water during 1999–2017 revealed by merging radiometer, scatterometer and model estimations, Remote Sens. Environ., 232, 111219, doi:10.1016/j.rse.2019.111219, 2019.

Zwally, H. J.: Microwave Emissivity and Accumulation Rate of Polar Firn, J. Glaciol., 18(79), 195–215, doi:10.3189/S0022143000021304, 1977.

Zwally, H. J. and Fiegles, S.: Extent and duration of Antarctic surface melting, J. Glaciol., 40(136), 463–475, doi:10.1017/S0022143000012338, 1994.

Zwally, H. J., Abdalati, W., Herring, T., Larson, K., Saba, J. and Steffen, K.: Surface Melt-Induced Acceleration of Greenland Ice-Sheet Flow, Science, 297(5579), 218–222, doi:10.1126/science.1072708, 2002.

Table 1. Annual mean and standard deviation of pan-Antarctic ~~melt onset~~EMO, CMO, melting days and MDF derived by AMSR-E/2 and ERA.

	~~Regions~~	~~WS~~	~~IO~~	~~PO~~	~~RS~~	~~BAS~~	~~AIS~~	~~All~~
~~AMSR-E/2~~	~~Melt onset (DOY)~~	~~19 Sep (81)±8~~	~~18 Sep (80)±7~~	~~30 Aug (61)±10~~	~~6 Sep (68)±8~~	~~10 Aug (41) ±14~~	~~4 Dec (158)±6~~	~~19 Sep (81)±5~~
	~~Melting days (days)~~	~~37±4~~	~~23±4~~	~~36±5~~	~~33±5~~	~~40±5~~	~~26±3~~	~~32±3~~
	~~MDF (%)~~	~~16±1~~	~~12±2~~	~~15±1~~	~~14±1~~	~~18±1~~	~~7±1~~	~~14±1~~
~~ERA~~	~~Melt onset (DOY)~~	~~11 Sep (73)±10~~	~~16 Sep (78)±17~~	~~26 Aug (57)±14~~	~~24 Aug (55)±9~~	~~29 Jul (29) ±10~~	~~3 Dec (157)±5~~	~~13 Sep (75)±6~~
	~~Melting days (days)~~	~~49±3~~	~~26±5~~	~~41±5~~	~~50±3~~	~~56±6~~	~~26±2~~	~~42±2~~
	~~MDF (%)~~	~~21±1~~	~~14±2~~	~~16±2~~	~~22±2~~	~~26±2~~	~~7±1~~	~~18±1~~

Observation	Melt index	WS	IO	PO	RS	BAS	AIS	All
AMSR-E/2	EMO (DOY)	24 Sep (86)±8	22 Sep (84)±6	4 Sep (66)±10	11 Sep (73)±8	15 Aug (46) ±15	7 Dec (160)±6	24 Sep (86)±5
	CMO (DOY)	12 Nov (135)±7	19 Nov (142)±5	15 Nov (138)±6	14 Nov (137)±10	5 Nov (128) ±12	18 Dec (171)±3	16 Nov (139)±4
	Melting days (days)	34±3	21±4	34±4	30±4	37±4	25±3	30±2
	MDF (%)	15±1	11±1	14±1	13±1	17±1	7±1	13±1
ERA	EMO (DOY)	9 Sep (71)±11	16 Sep (78)±16	25 Aug (56)±14	23 Aug (54)±9	28 Jul (28) ±10	3 Dec (156)±5	12 Sep (74)±6
	CMO (DOY)	22 Oct (114)±11	9 Nov (132)±10	22 Oct (114)±12	29 Sep (91)±10	7 Sep (69) ±16	10 Dec (163)±6	20 Oct (112)±7
	Melting days (days)	49±3	26±4	41±5	50±3	56±6	26±2	42±2
	MDF (%)	21±1	13±2	16±2	22±2	26±2	7±1	18±1

Table 2. Trends ~~of snowmelt onset~~in pan-Antarctic EMO, CMO, melting days and MDF during 2002-2017. Trends with *, ** and * indicate statistical significance at 90%, 95%, and 99% confidence levels, respectively. The uncertainties of the trends were estimated at 90% confidence level.**

~~Regions~~	~~WS~~	~~IO~~	~~PO~~	~~RS~~	~~BAS~~	~~AIS~~	~~All~~
~~Melt onset (days yr^{-1})~~	~~-0.39~~	~~0.30~~	~~1.44*~~	~~1.65***~~	~~2.13**~~	~~0.79~~	~~0.70**~~
~~Melting days (days yr^{-1})~~	~~0.22~~	~~0.17~~	~~0.47~~	~~-0.69**~~	~~-0.39~~	~~-0.35~~	~~-0.07~~
~~MDF (% yr^{-1})~~	~~0.17~~	~~0.08~~	~~0.06~~	~~-0.20**~~	~~-0.12~~	~~-0.10~~	~~0.02~~

Melt index	WS	IO	PO	RS	BAS	AIS	All
EMO (days yr^{-1})	-0.35±1.10	0.09±0.82	1.37±1.40	1.72±0.71***	2.13±1.88*	0.71±0.76	0.68±0.59*
CMO (days yr^{-1})	-0.82±0.72*	-0.84±0.51**	-0.16±0.71	0.52±1.23	0.59±1.74	0.22±0.51	-0.22±0.43
Melting days (days yr^{-1})	0.34±0.33*	0.37±0.42	0.80±0.46***	-0.52±0.43*	-0.05±0.57	-0.33±0.41	0.11±0.20
MDF (% yr^{-1})	0.20±0.14**	0.15±0.14*	0.19±0.12**	-0.14±0.14	0.02±0.19	-0.09±0.11	0.07±0.08

Table 3. Correlation between snowmelt index and atmospheric index for the Period 2002–2017. Correlation coefficients with *, ** and * indicate statistical significance at 90%, 95%, and 99% confidence levels, respectively.**

Atmospheric index	Melt index	WS	IO	PO	RS	BAS	AIS	All
SAM	EMO	-0.27	0.77***	0.32	0.16	0.25	0.52*	0.31
	CMO	-0.03	0.15	0.03	0.50*	0.53*	0.80***	0.54**
	Melting days	0.37	0.18	0.01	-0.26	-0.42	-0.88***	-0.02
	MDF	0.18	-0.11	-0.07	-0.48*	-0.53*	-0.88***	-0.33
SOI	EMO	0.11	-0.08	-0.01	0.10	0.28	0.55**	0.19
	CMO	0.09	-0.23	0.14	-0.53*	-0.12	0.18	-0.31
	Melting days	0.03	-0.26	0.07	-0.11	0.46*	-0.03	-0.07
	MDF	-0.16	-0.18	0.12	0.15	0.34	-0.03	-0.09
Nino3.4	EMO	-0.28	-0.06	-0.11	-0.02	-0.26	-0.47*	-0.27
	CMO	-0.15	0.19	-0.35	0.66**	0.28	0.01	0.35
	Melting days	0.04	0.42	-0.16	0.08	-0.54**	-0.15	-0.07
	MDF	0.24	0.36	-0.11	-0.22	-0.46*	-0.15	0.13

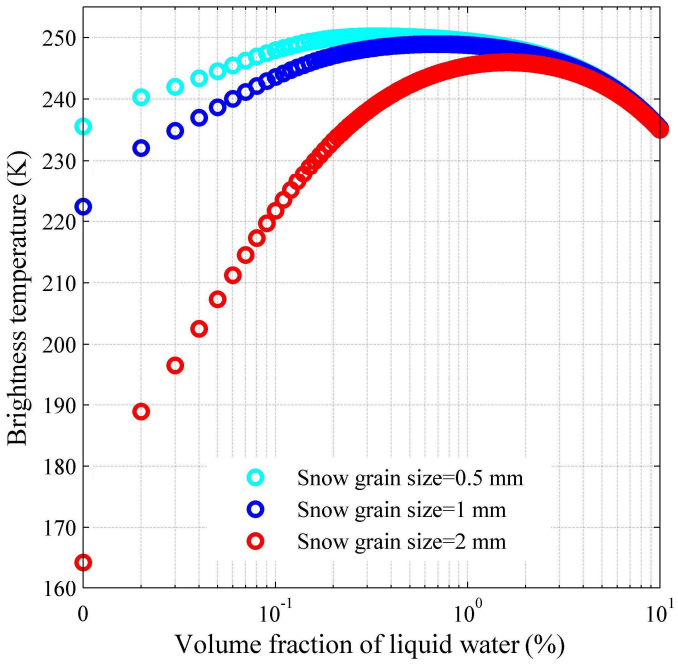

Figure 1. Simulated Tb_{V36} varying with liquid water when the snow grain size is 0.5 cm (cyan), 1 mm (blue) and 2 mm (red).

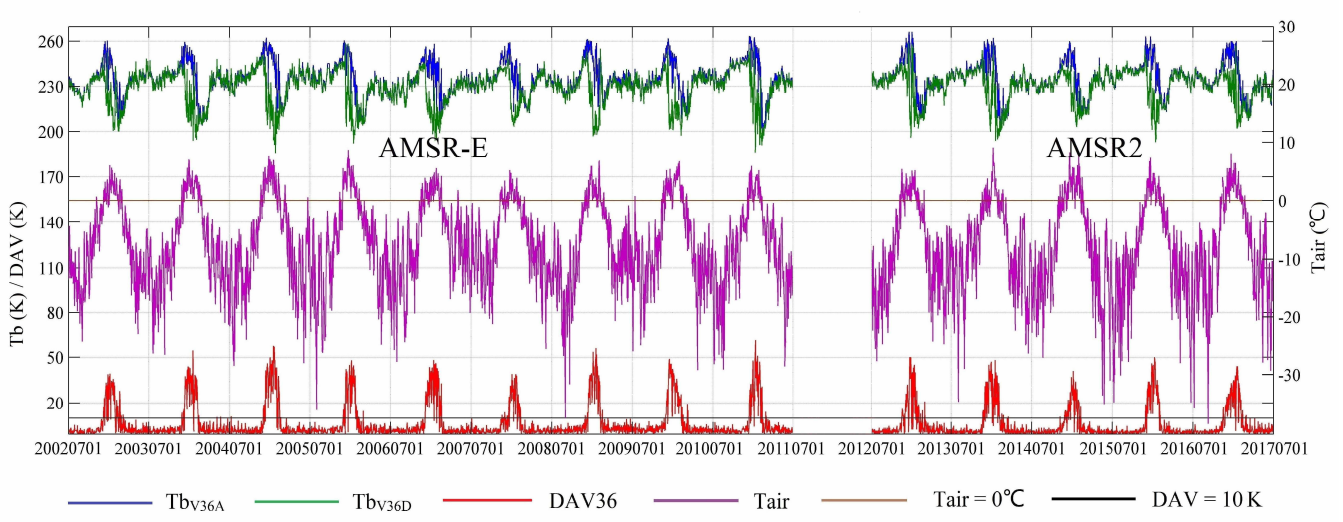

Figure 2. The comparison between Tair and satellite observations (AMSR-E from 2002 to 2011 and AMSR2 from 2012 to 2017) at Zhongshan Station, including daily maximum Tair (purple line), Tb_{V36A} (dark blue line), Tb_{V36D} (dark green line) and DAV36 (red line); Brown and black lines represent Tair = 0℃ and DAV = 10 K.

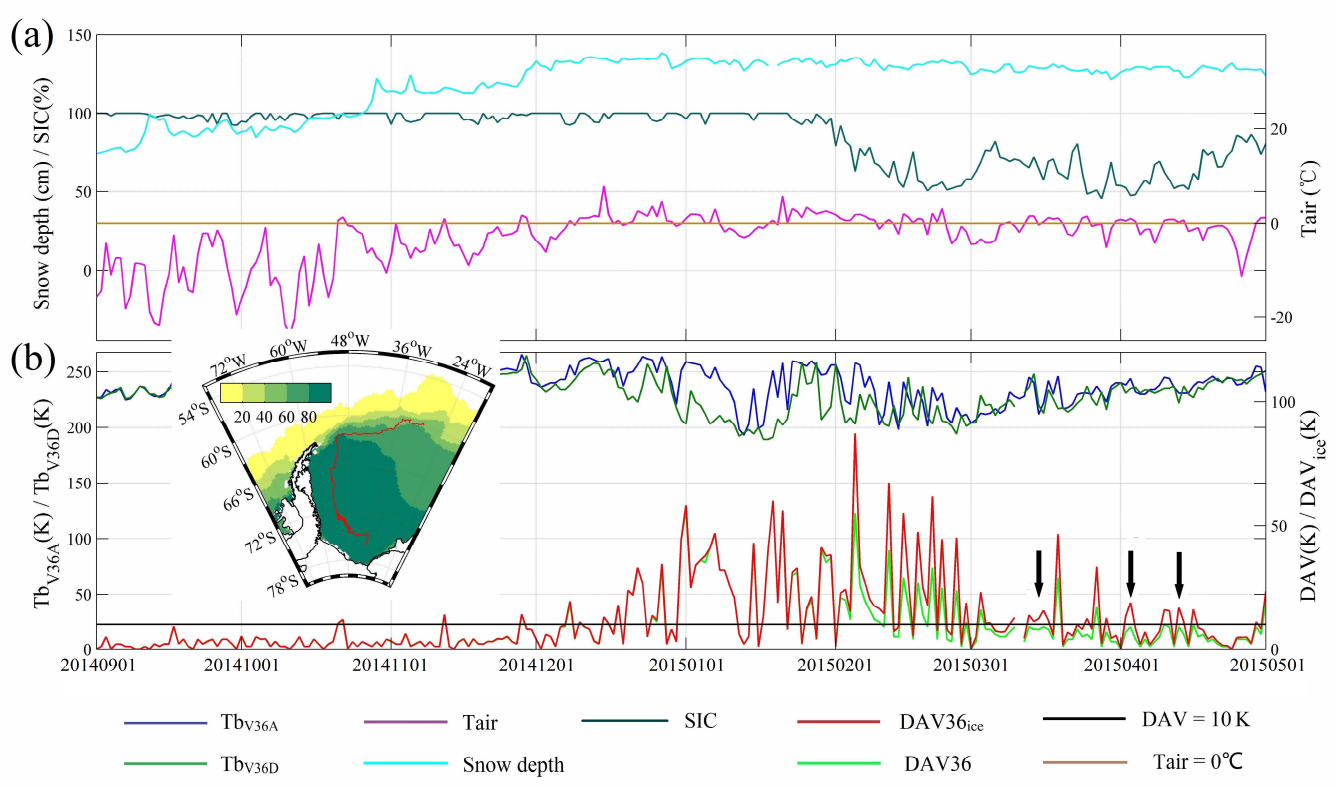

Figure 3. Meteorological and satellite measurements along a sea ice buoy in the Weddell Sea from 1 September, 2014 to 1 May, 2015. (a) Snow depth (cyan line), daily maximum Tair (pink line), and SIC (olive line); the brown line represents Tair = 0°C. (b) Tb_{V36A} (dark blue line), Tb_{V36D} (dark green line), DAV36 (light green line) and $DAV36_{ice}$ (red line); the black line represents DAV=10 K. The inset map in (b) illustrates the annual mean SIC and the route of the buoy from multi-year ice to first-year ice. The black arrows indicate the cases that melt events were recognized by $DAV36_{ice}$ rather than DAV36.

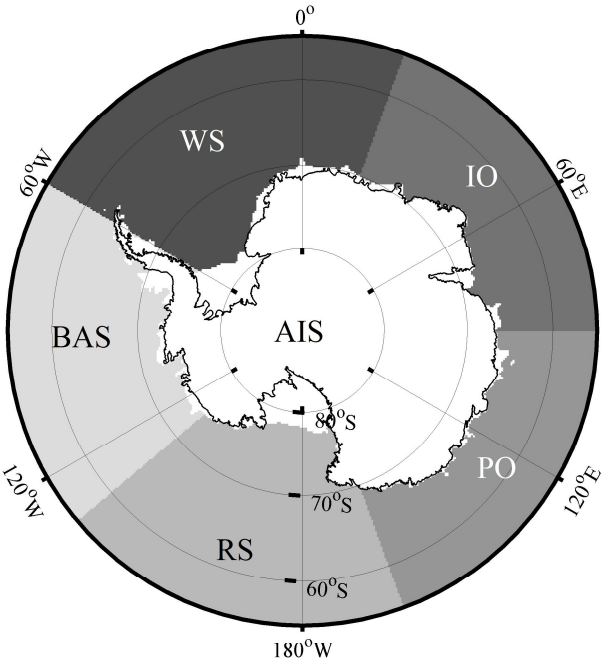

WS-*Weddell Sea* **IO**-*Indian Ocean* **PO**-*Pacific Ocean* **RS**-*Ross Sea*

BAS-*Bellingshausen Amundsen Sea* **AIS**-*Antarctic ice sheet*

Figure 4. Map of the different regions across the ~~P~~pan-Antarctic.

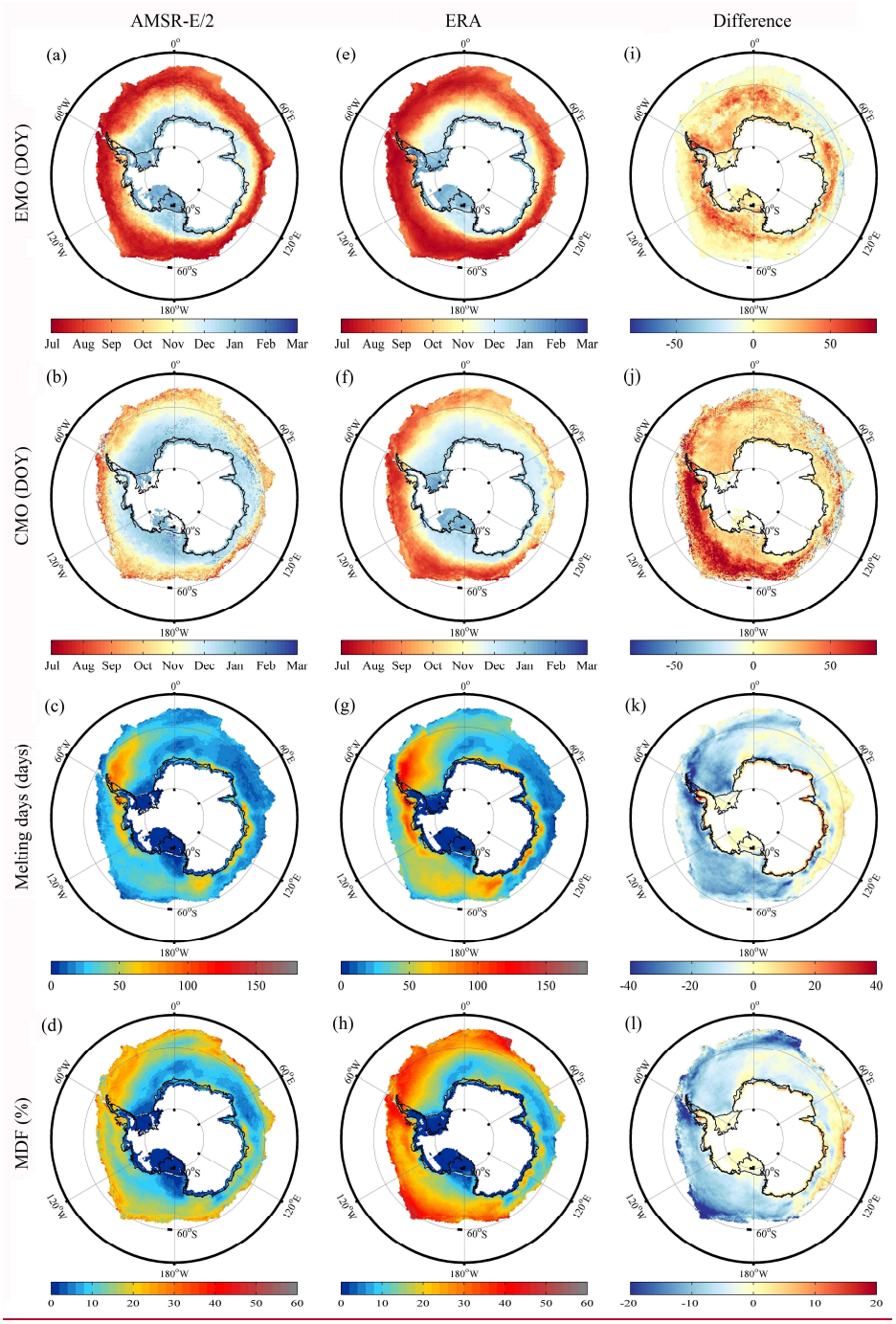

Figure 5. Annual mean EMO, CMO, melting days and MDF derived by AMSR-E/2 (a-d) and ERA (e-h), also shown are the differences (AMSR-E/2 minus ERA) between the two observations (i-l).

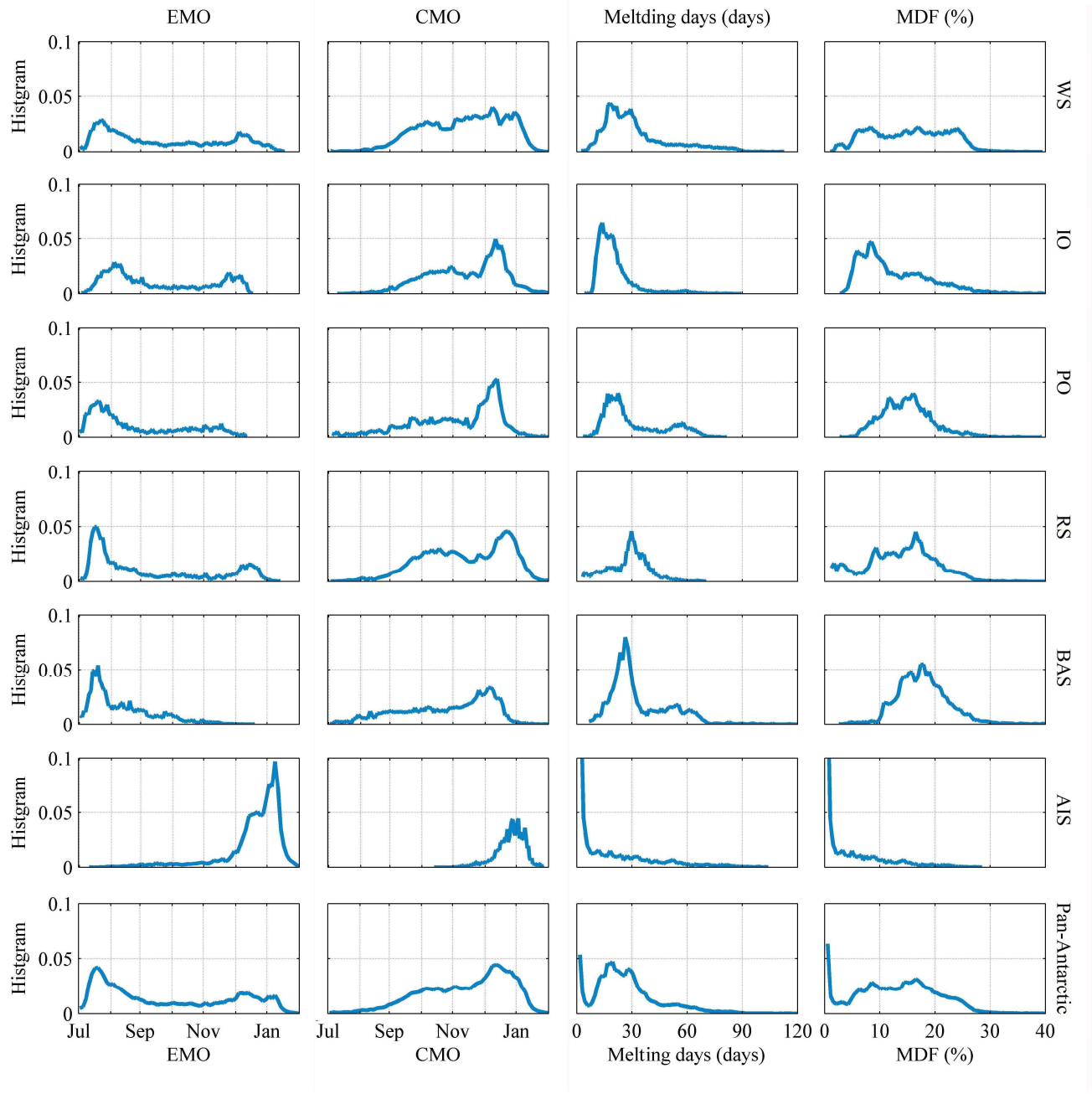

Figure 6. Normalized histograms of annual mean EMO, CMO, melting days and MDF for pan-Antarctic and different regions.

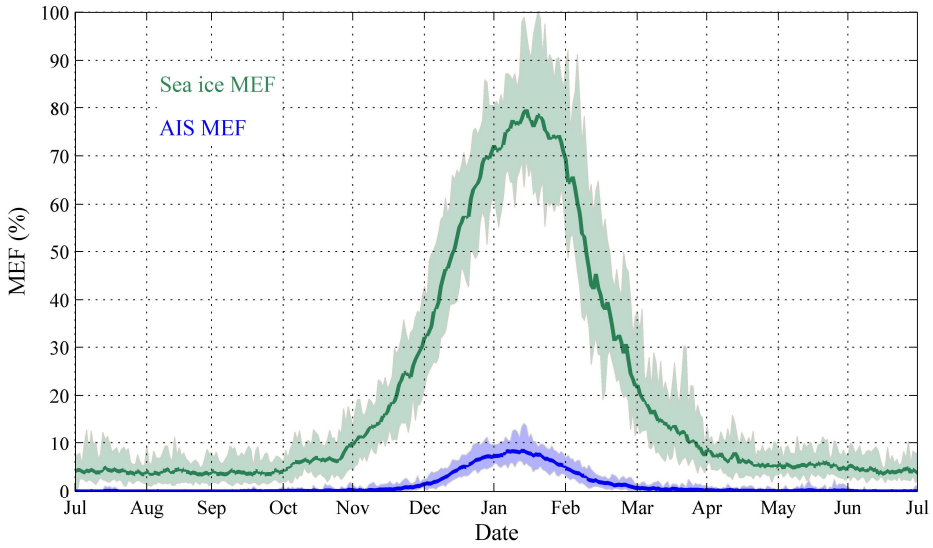

Figure 7. Daily mean Antarctic sea ice MEF and AIS MEF, the corresponding shadows indicate daily maximums and minimums.

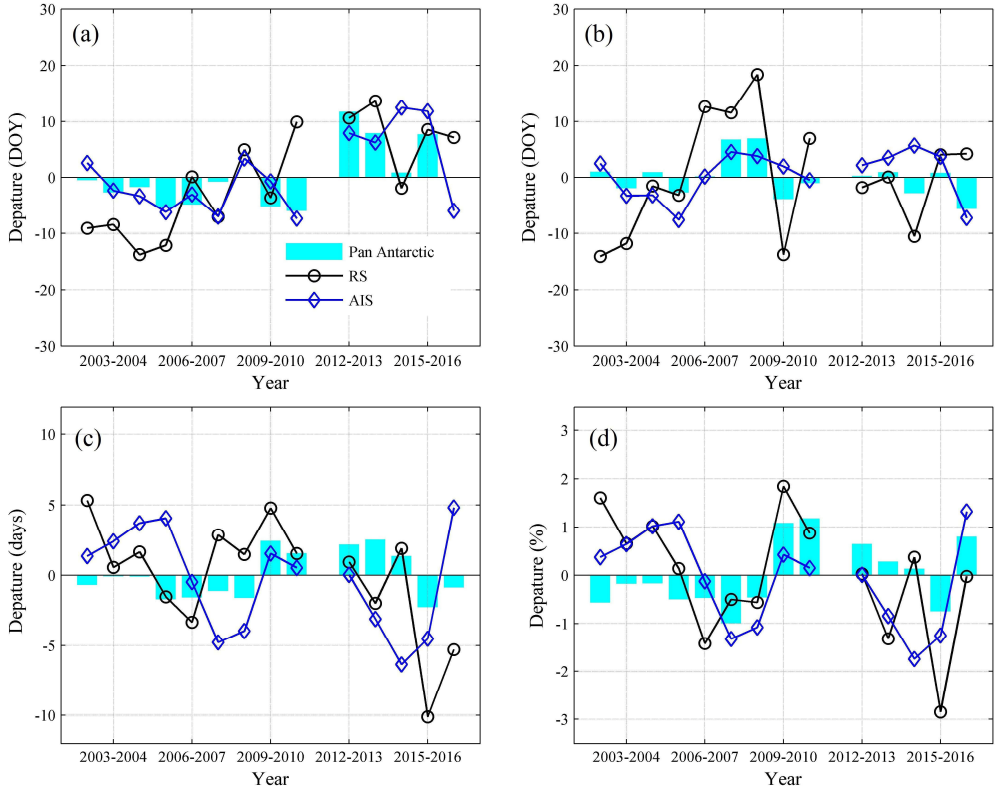

Figure 8. Departure of annual mean (a) EMO, (b) CMO, (c) melting days and (d) MDF for the pan-Antarctic, RS and the AIS.

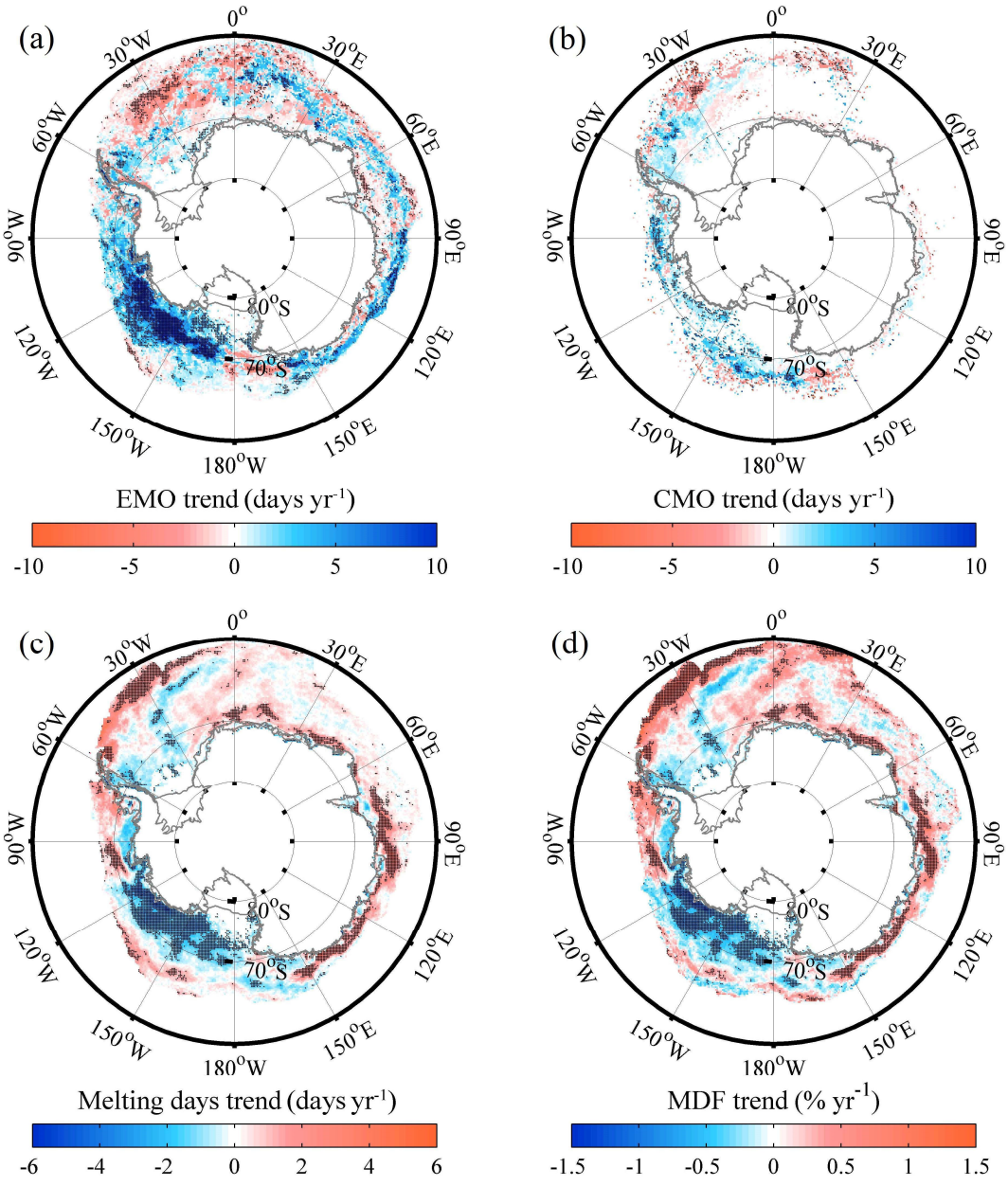

Figure 9. Trends in (a) EMO (b) CMO, (c) melting days and (d) MDF, black points indicate the pixels with trends above 90% confidence level.

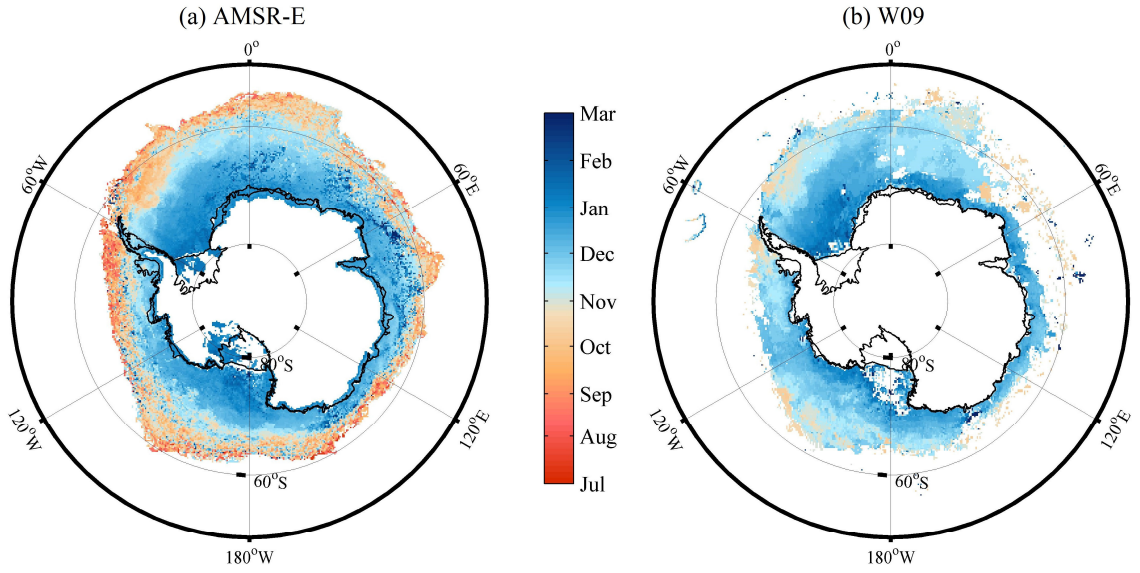

Figure 10. Annual mean CMO derived from (a) AMSR-E and (b) W09 from 2002 to 2008.

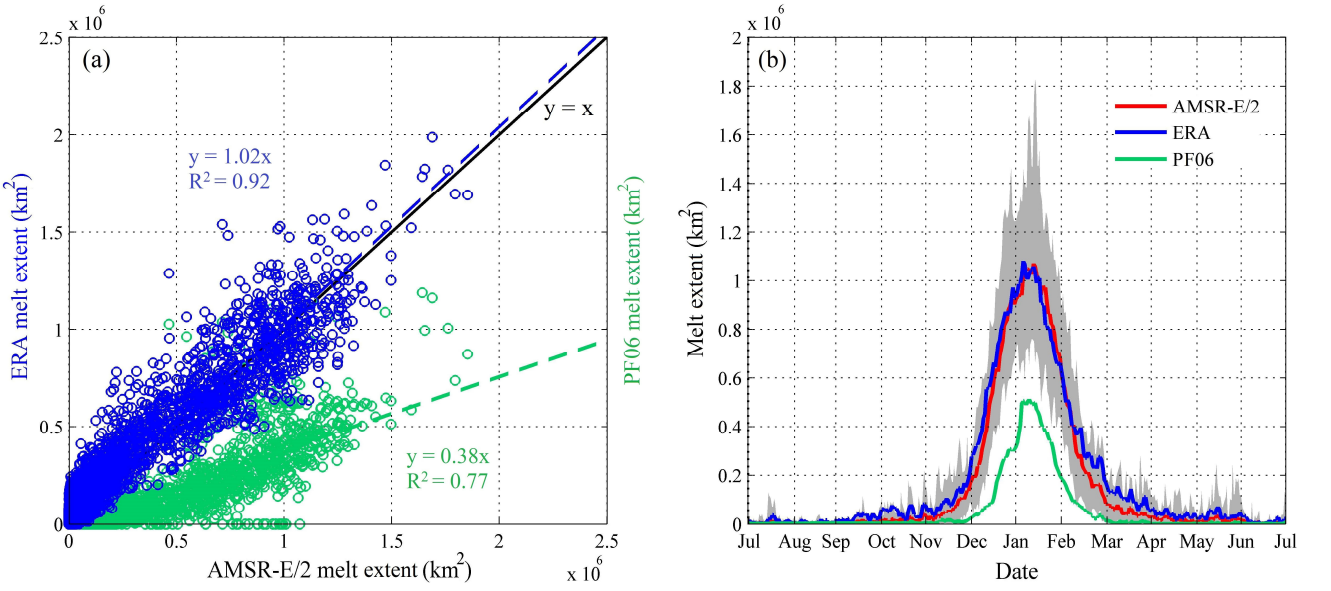

Figure 11. Comparison of AIS melt extent derived by AMSR-E/2, ERA, and PF06 from 2002 to 2017. (a) Scatter plot of daily melt extent, blue circles indicate AMSR-E/2 vs. ERA and green circles indicate AMSR-E/2 vs. PF06. (b) Daily mean melt extent derived by AMSR-E/2 (red line), ERA (blue line) and PF06 (green line), grey shadow indicates the daily maximum and minimum melt extent detected by AMSR-E/2.

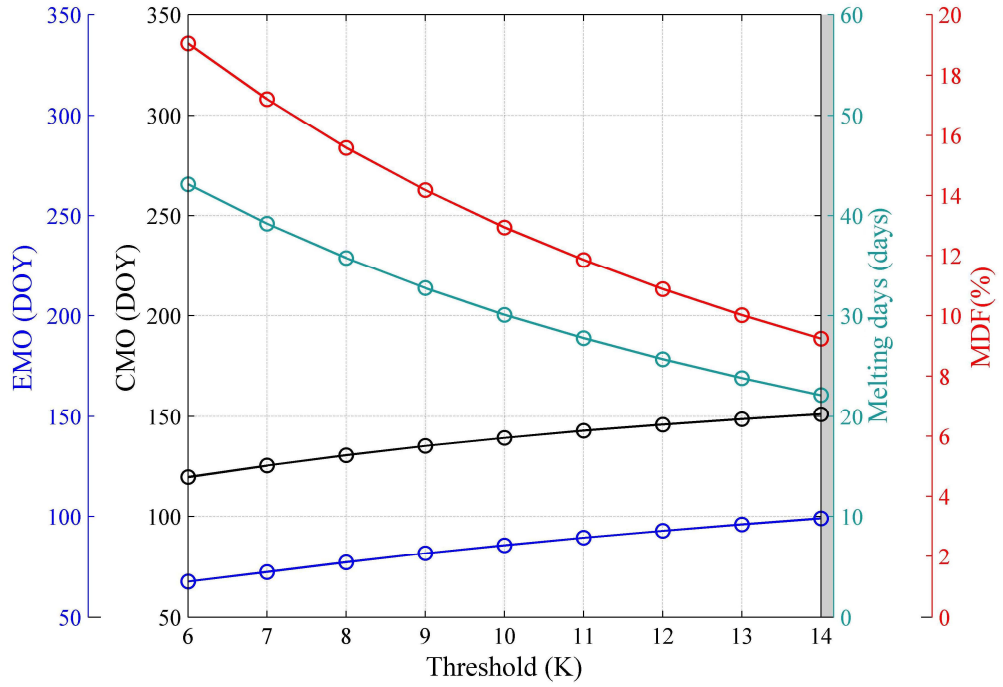

Figure 12. Annual mean EMO (blue dots), CMO (black dots), melting days (cyan dots) and MDF (red dots) with the threshold for AMSR-E/2 DAV36 varying from 6-14 K.

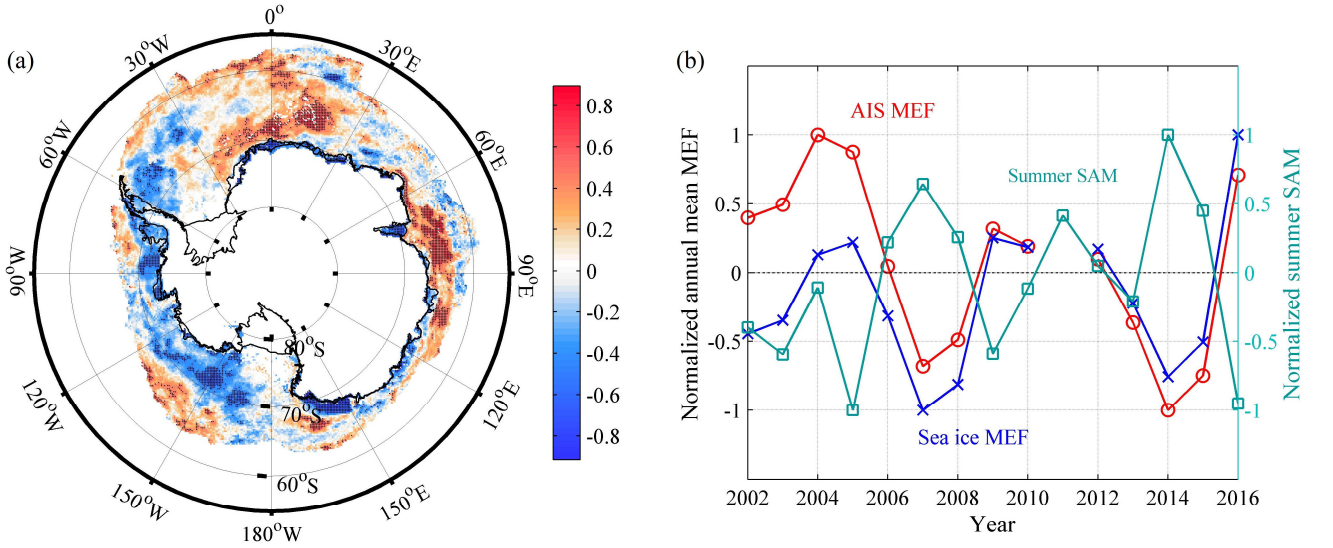

Figure 13. Linkage between pan-Antarctic snowmelt and summer SAM. (a) Correlation coefficient between MDF and summer SAM, black points indicate the trends above 90% confidence level. (b) Comparison of normalized summer SAM (cyan line), normalized annual mean Antarctic sea ice MEF (blue line) and AIS MEF (red line).

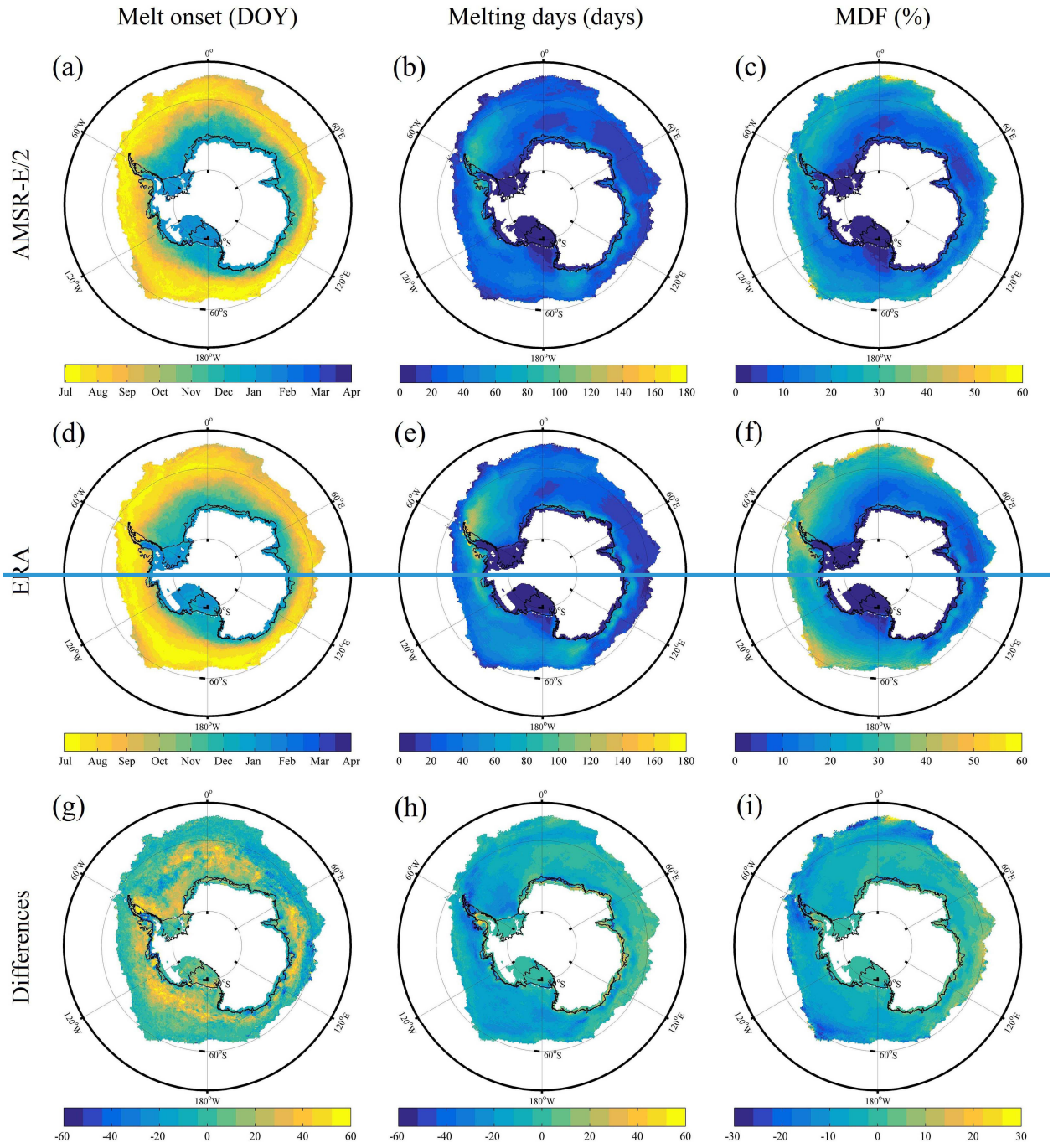

~~**Figure 5. Annual mean melt onset, melting days and MDF derived by AMSR-E/2 (a-c) and ERA (d-f), also shown are the differences (AMSR-E/2 minus ERA) between the two observations (g-i).**~~

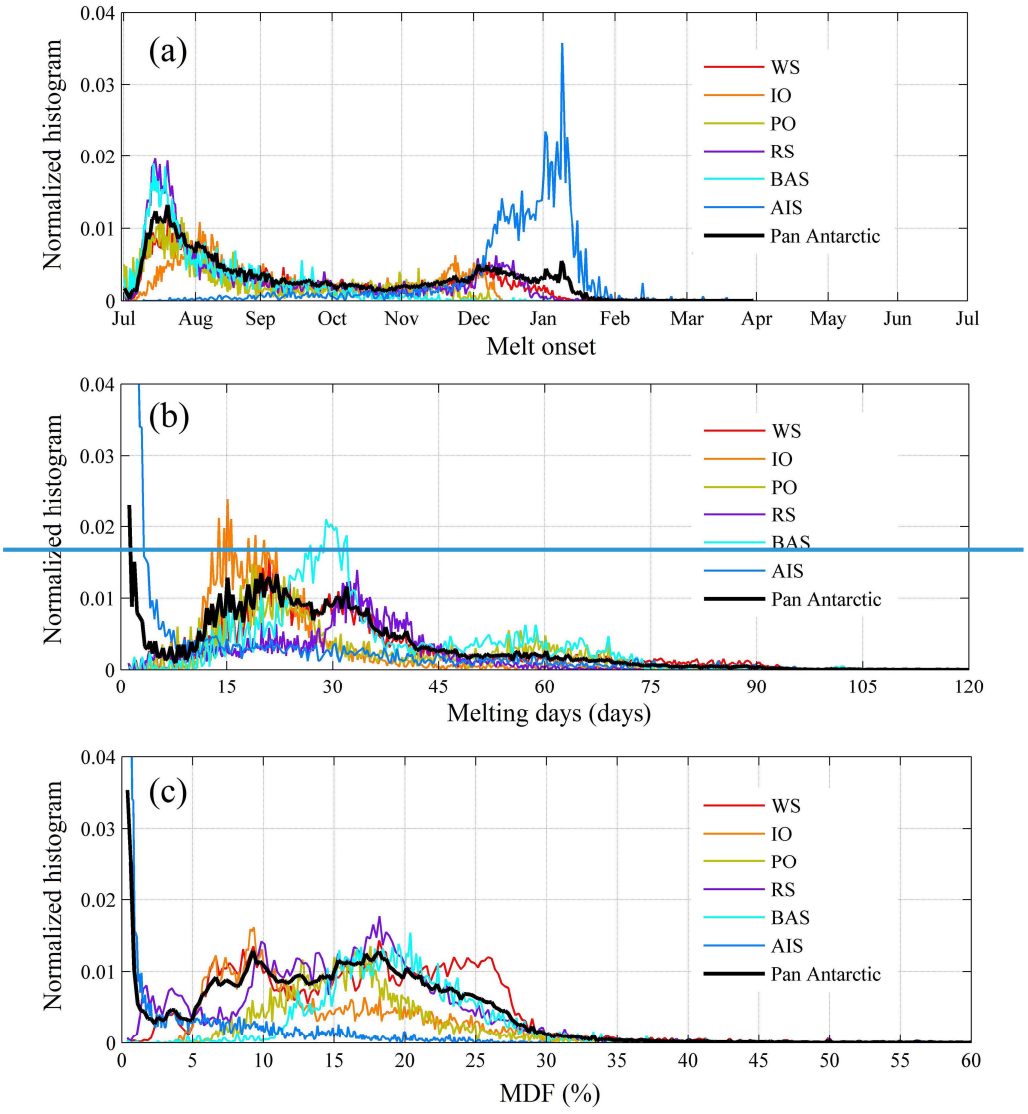

Figure 6. Distributions of annual mean (a) melt onset, (b) melting days and (c) MDF derived by AMSR-E/2.

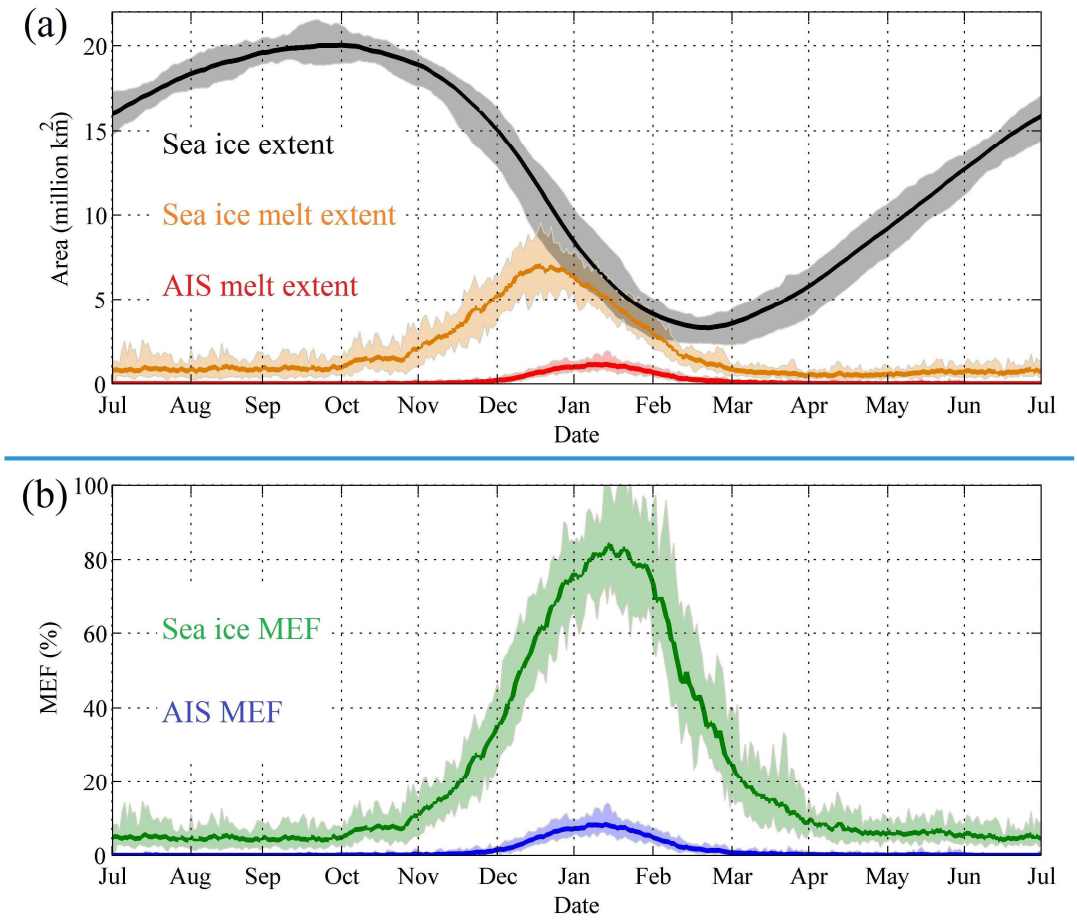

~~Figure 7. Melt extent and MEF in the pan-Antarctic. (a) Daily mean sea ice extent (black line), sea ice melt extent (brown line) and AIS melt extent (red line); (b) daily mean sea ice MEF (green line) and AIS MEF (blue line); the corresponding shadows indicate daily maximums and minimums.~~

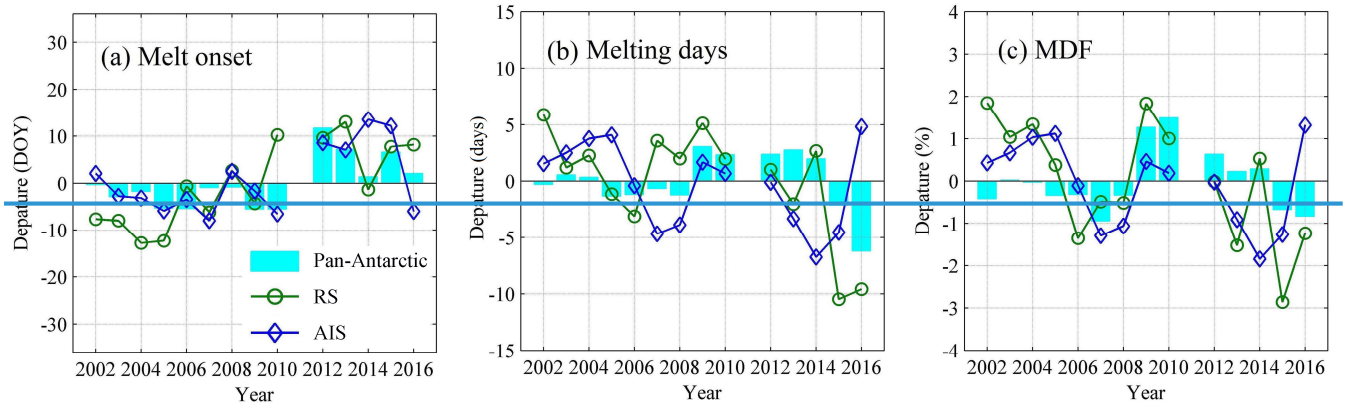

~~Figure 8. Departure of annual mean (a) melt onset, (b) melting days and (c) MDF for the pan-Antarctic (cyan bar), RS (green line) and the AIS (blue line).~~

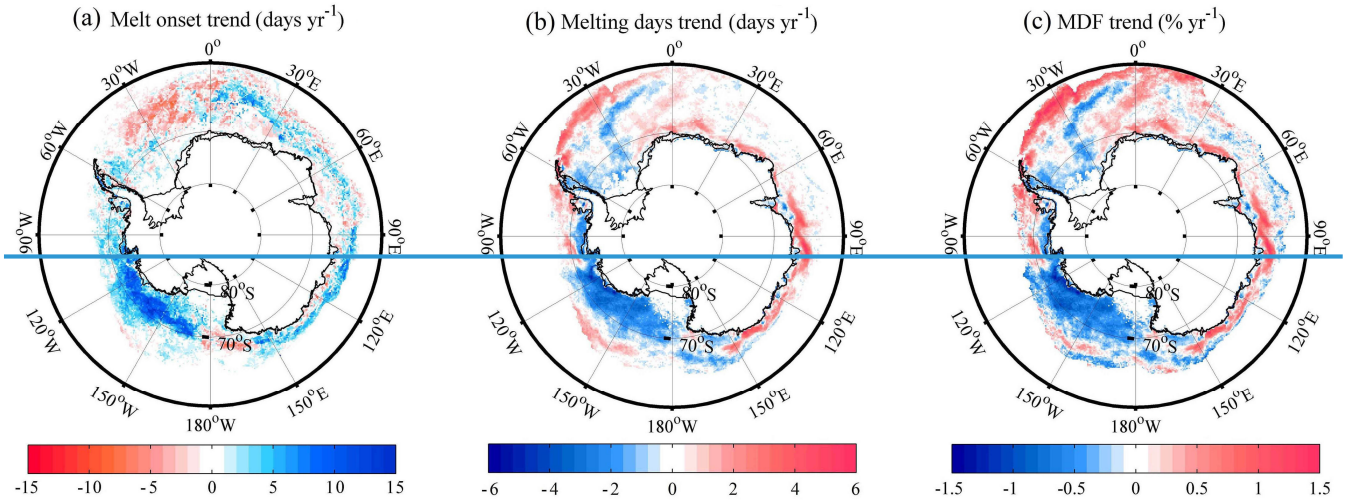

~~Figure 9. Map shows the trend in (a) melt onset, (b) melting days and (c) MDF.~~

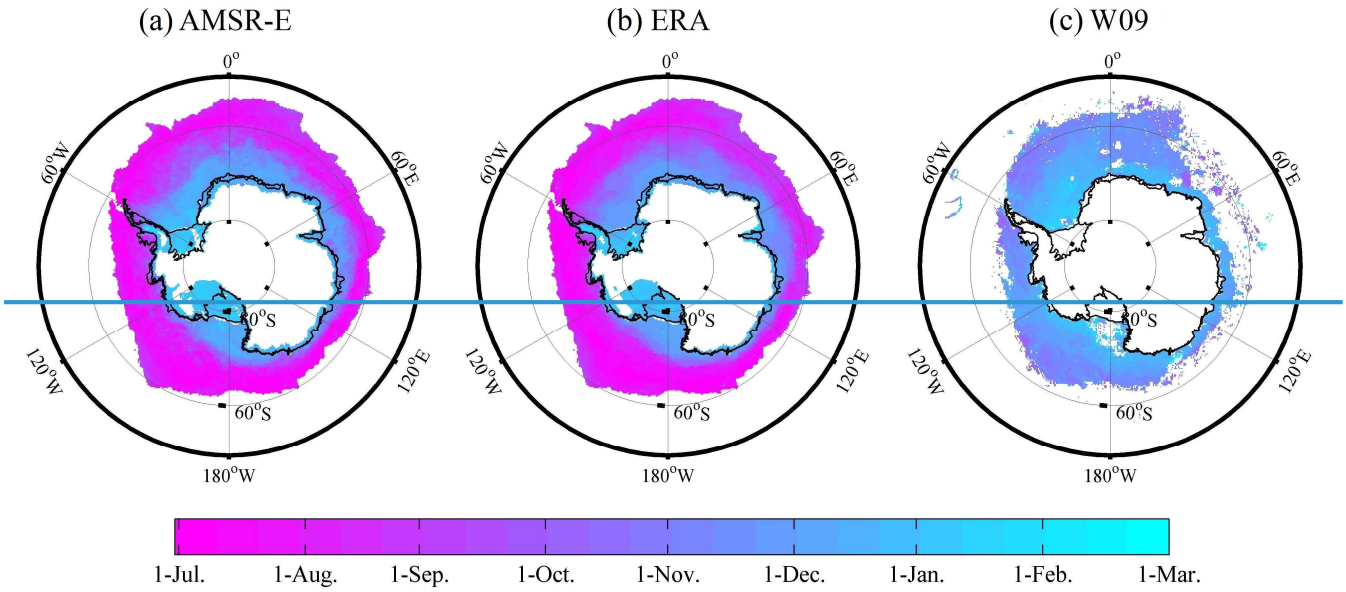

~~Figure 10. Annual mean melt onset derived from (a) AMSR-E, (b) ERA (middle) and (c) W09 from 2002 to 2008.~~

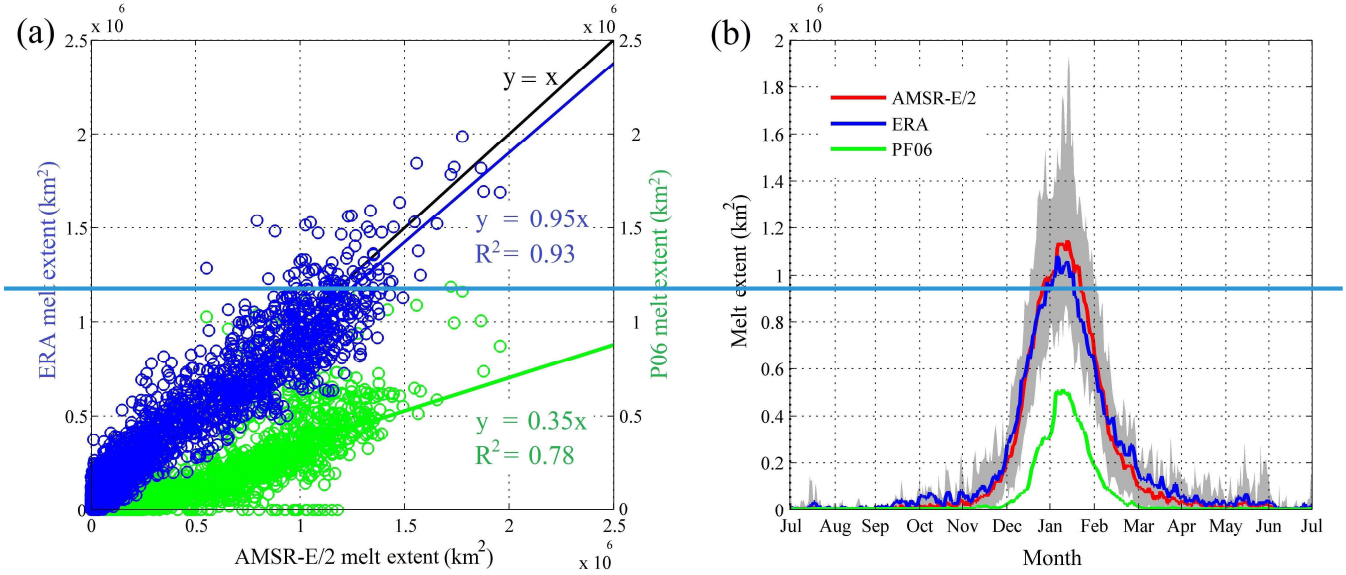

~~Figure 11. Comparison of AIS melt extent derived by AMSR-E/2, ERA, and PF06 from 2002 to 2017. (a) Scatter plot of daily melt extent, blue circles indicate AMSR-E/2 vs. ERA, and green circles indicate AMSR-E/2 vs. PF06. (b) Daily mean melt extent derived by AMSR-E/2 (red line), ERA (blue line) and PF06 (green line), grey shadow indicates the daily maximum and minimum melt extent detected by AMSR-E/2.~~

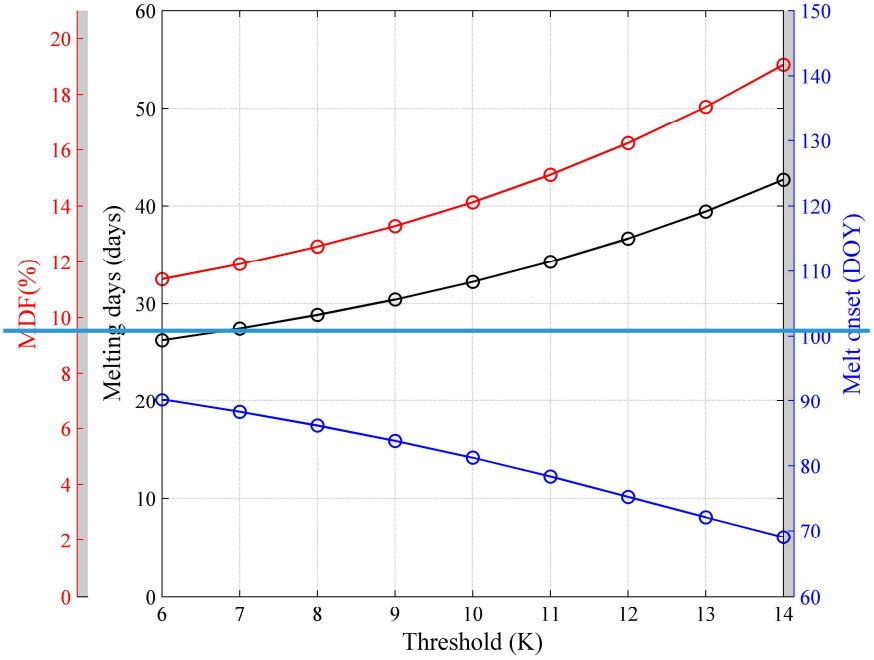

~~Figure 12. Annual mean melt onset (blue dots), melting days (black dots) and MDF (red dots) with the threshold for AMSR-E/2 DAV36 varying from 6-14 K.~~

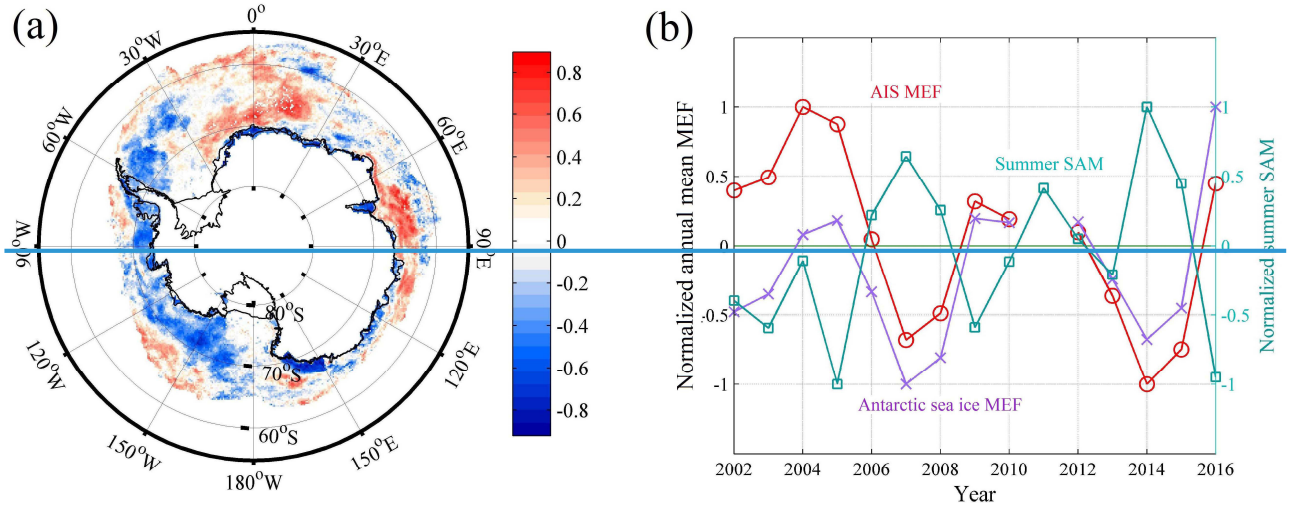

~~Figure 13. Linkage between Pan-Antarctic snowmelt and summer SAM. (a) Correlation coefficient between MDF and summer SAM. (b) Comparison of normalized summer SAM (cyan line), normalized annual mean Antarctic sea ice MEF (purple line) and AIS MEF (red line).~~